°MSc

HELSINKI UNIVERSITY OF TECHNOLOGY
Electronics and Electrical Engineering

Jenny Vesterlund

LIGHT ADAPTATION IN MOUSE CONES

Espoo 15.01.2009

Thesis supervisor:

Prof. Ari Koskelainen

Thesis instructor:

DI Hanna Heikkinen

HELSINKI UNIVERSITY OF TECHNOLOGY

Author: Jenny Vesterlund

Title: Light adaptation in mouse cones

Date: 15.01.2009 Language: English Number of pages: 11+62

Department: Faculty of Electronics, Communications and Automation

Professorship: Medical Engineering Code: Tfy-99

Supervisor: Prof. Ari Koskelainen

Instructor: DI Hanna Heikkinen

The rod photoreceptors are used for twilight vision and are saturated in daylight. Cones function in daylight and have not been found to saturate at any intensity available. Both rods and cones have the ability to regulate their operation as a function of the background illumination so as to extend their operational functioning range. General light adaptation manifestations can be observed as photoreceptor desensitization and photoresponse acceleration. In this study the function of cone light adaptation was studied.

The electrophysiological changes in mouse cones caused by light adaptation were recorded as mass potential electroretinograms (ERG). The photoreceptor's response to light was pharmacologically isolated. In one case, the retinae were subjected to short stepped backgrounds (test flash applied 2 s after background onset) and in the othe case continuous backgrounds (test flash applied more than 2 min. after background onset). Characteristics of mouse cone light adaptation include retardation in time to maximum (t_p) in both types of backgrounds. The sensitivity drop in the photoreceptors when subjected to increasingly stronger stepped background illumination was smaller than in the continuous background. The results obtained in these experimental conditions indicate that light adaptation functions differently in mouse cones compared to other species.

Additionally, a mouse lacking functional rod phototransduction, due to targeted deletion of α transducin gene (Tr$\alpha-/-$), was investigated in order to determine whether the Tr$\alpha-/-$ mouse could be used as a model for cone phototransduction experiments. The photoresponse kinetics of the Tr$\alpha-/-$ photoreceptors, though, were significantly retarded. Furthermore, the Tr$\alpha-/-$ photoreceptors were somewhat more light sensitive than WT mouse cones, and highly more sensitive to adapting background illumination.

Keywords: Cone, Light Adaptation, Mice, ERG, α- transducin knockout

TEKNISKA HÖGSKOLAN

Författare: Jenny Vesterlund

Arbetets namn: Ljudadaptation i möss tappar

Datum: 15.01.2009 Språk: Engelska Sidmängd: 11+62

Fakultet: Fakulteten för elektronik, kommunikation och automation

Professur: Medicinsk teknik Kod: Tfy-99

Övervakare: Prof. Ari Koskelainen

Handledare: DI Hanna Heikkinen

De fotoreceptorer, som kallas stavar, används för mörkersyn och är mättade i dagsljus. Den andra typen av receptor, tappen, funktionerar i dagsljus och man har inte funnit att den mättas vid någon tillgänglig ljusintensitet. Såväl stavar som tappar kan reglera sin funktion som en funktion av bakgrundsintensiteten. Detta för att kunna funktionera över ett större intensitetsspektrum. De allmänna karaktärsdragen för fotoreceptorernas ljusadaptation kan observeras som minskning i receptorns känslighet samt acceleration av fotosvaret. I denna studie har tapparnas ljusadaptation undersökts.
De elektrofysiologiska förändringarna i möss tappar som beror på ljusadaptation registrerades som masspotential elektroretinogram (ERG). Fotoreceptorernas svar på ljus isolerades farmakologiskt.
Näthinnorna utsattes antingen för bakgrundsillumination (icke kontinuerlig, stimulusljuset applicerades 2 s efter bakgrundsljuset tänts) eller kontinuerlig bakgrundsillumination (stimulusljuset applicerades 2 min efter bakgrundsljuset tänts). Resultaten indikerar att möss tappars ljusadaptation manifesteras som en retardation av t_p (tid till maximum) i båda typerna av bakgrund. Resultaten från denna studie indikerar att ljusadaptationen fungerar olika i möss tappar jämfört med andra djurarters tappar.
Därutöver undersöktes en mus, som saknade fungerande stav-fototransduktion (Tr$\alpha -/-$), för att avgöra huruvida denna Tr$\alpha -/-$ mus skulle kunna användas som en modell för experiment av tappars fototransduktionsfunktion. Fotosvaren var dock betydligt långsammare. Därtill var Tr$\alpha -/-$-fotoreceptorerna något mera ljuskänsliga jämfört med möss (av vild typ) samt betydligt mera känslig för adapterande bakgrundsillumination.

Nyckelord: Kon, ljusadaptation, möss, ERG, α- transducin knockout

Preface

Jag vill nu ta tillfället i akt och tacka min professor Ari Koskelainen för att ha gett mig ett intressant och utmanande ämne. Tack vare detta har jag fått pressa mig själv att göra ett bättre jobb än vad jag annars skulle ha gjort. Därtill vill jag tacka min handledare Hanna för att tagit sig den tid det behövdes för att hjälpa mig och orkat förklara hur saker och ting fungerar. Men även alla andra kolleger, Soile, Frans, Janne, Elina samt Anna, på vårt labb förtjänar sitt tack. Alla har gjort sitt för att skapa en trevlig stämning där det har varit trevligt att jobba. Soile förtjänar dock ett speciellt tack. Hon är verkligen en speciell person, som alltid är villig att lyssna och motivera när det känns som tyngst. Sist och slutligen vill jag även tacka vänner och familj för att ni orkat lyssna på mina ibland långrandiga förklaringar om hur ögat funkar och för att ni alla varit ett stöd under denna tid.

Närpes, 15.01.2009

Jenny Vesterlund

Contents

Abstract ii
Abstract (in Swedish) ii
Preface iv
Contents v
Symbols, Abbreviations, and Glossary viii

1 Introduction **1**

2 The Vertebrate Eye and Phototransduction **4**
2.1 The Vertebrate Eye and Seeing 4
2.2 The Retina 5
2.2.1 Photoreceptors 5
2.3 Phototransduction 8
2.3.1 Dark-adapted Transretinal Current 8
2.3.2 Activation of Phototransduction 9
2.3.3 Deactivation and Regeneration of Signaling Molecules . . . 10

3 Light Adaptation **13**
3.1 Calcium Dependent Mechanisms of Light Adaptation 15
3.1.1 Regulation of Guanylate Cyclase Activity 15
3.1.2 Regulation of CNG-Channel Affinity 15
3.1.3 Calcium Buffering 16
3.1.4 Regulation of PDE-activity 16
3.2 Light Adaptation Mechanisms Independent of Calcium 17
3.2.1 Response Compression 17
3.2.2 Steady-state PDE-activity 17
3.2.3 Protein Translocation 17

3.3 Light Adaptation in Cones . . . 17
3.3.1 Pigment Bleaching . . . 18
3.3.2 Protein Translocation . . . 18

4 Photoresponses and the Electroretinogram **19**
4.1 The Components of the Photoresponse . . . 19
4.1.1 The a-wave and fast PIII component . . . 22
4.1.2 The b-wave . . . 22
4.1.3 The c-wave . . . 23
4.1.4 The Slow PIII . . . 23
4.1.5 The Nose Component . . . 24

5 Methods **25**
5.1 Preparations and Solutions . . . 25
5.1.1 Solutions . . . 25
5.1.2 The ERG-apparatus . . . 25
5.1.3 Determining the Stimulus Intensities and the Number of R* produced in Rods . . . 29
5.1.4 Determining of the Number of R* Produced in Cones . . . 29
5.2 The Photoresponses . . . 31
5.2.1 Isolation of the Photoreceptor Component . . . 31
5.2.2 Separation the Rod and Cone Responses . . . 31
5.2.3 General Photoresponse Properties . . . 32
5.3 The Recording Protocols . . . 33
5.3.1 The Stimulus Protocols . . . 34
5.4 Analysis . . . 35
5.4.1 Fractional Responses . . . 35
5.4.2 Amplitude vs. intensity plots . . . 35
5.4.3 Dominant Time Constant of Recovery . . . 36

6 Results **37**
6.1 Dark adapted Rods and Cones . . . 37
6.2 Light-adapted Cones . . . 39
6.2.1 Stepped Background . . . 40
6.2.2 Continuous Backgrounds . . . 44

6.3 α-transducin Knockout Mouse 47
6.3.1 Dark Adapted Photoresponses 47
6.3.2 Light Adaptation of Tr$\alpha-/-$ Photoreceptors 48

7 Discussion **52**
7.1 Rod and Cone a-wave Characteristics 52
7.2 Light Adaptation 53
7.3 α-transducin Knockout Mouse 54
7.3.1 Dark-adapted Tr$\alpha-/-$ Photoreceptors 54
7.3.2 Light Adaptation of Tr$\alpha-/-$ Photoreceptors 55

Symbols, Abbreviations, and Glossary

Symbols

a_c	Photoreceptor end-on collecting area.
$[c]_i$	Intracellular concentration of molecule c.
$[c]_e$	Extracellular concentration of molecule c.
d	Diameter of photoreceptor outer segment.
D	The optical density of an material, i.e. the amount a material will attenuate the light passing through it.
f	Dimensionless factor that accounts for the light funneling by the photoreceptor inner segments.
Φ	The number of absorbed photons that gave rise to photoisomerization during a stimulation.
G/G*	An inactive/active G protein transducin.
γ	The quantum efficiency of the photoisomerization, i.e. how many absorbed photons that elicit a photoisomerization. by rods due to their position in the retina when illuminated
I_0	Unattenuated light intensity.
I_F	The stimulus light intensity after passing through the filters and wedges.
K_{cG}	The concentration of cGMP needed for half-maximal opening of the CNG-channels.
k_{shadow}	A corrective term that accounts for the shadowing of cones done by rods due to their position in the retina when illuminated from the pigment epithelial side.
l	Outer segment length of the photoreceptor.
λ	The wavelength of light.
λ_{max}	The wavelength of light that yields in the greatest absorption of photons.
PDE/PDE*	An inactive/active cGMP PDE molecule.
R/R*	An inactive/active photopigment.
S	Fractional sensitivity. Describes the fraction of photo current turned off by a single photoisomerization.
T	Temperature.
t_p	Time required for reaching maximum response amplitude.

Abbreviations

ADP	Adenosine diphospate.
$Ag/AgCl^{-}$	Silver/Silverchloride
ATP	Adenosine triphospate. The main energy source of the cell.
ATPase	Adenosine triphosphatase, an enzyme that start the process of hydrolyzing ATP to ADP.
cGMP	Cyclic guanosine monophosphate.
COS	Cone Outer Segment.
ERG	Electroretinogram.
GAP	GTPase accelerating protein.
GC	Guanylate cyclase. An enzyme that catalyzes the synthesis of cGMP.
GCAP	Guanylate cyclase Activating Protein.
GDP	Guanosine diphosphate.
GTP	Guanosine triphosphate.
GTPase	Guanosine triphosphatase, an enzyme that starts the process of hydrolyzing GTP to GDP.
IS	Inner Segment.
PDE	Phosphodiesterase.
RPE	Retinal pigment epithelium.
RGS	Regulators of G-protein signaling.
ROS	Rod outer segment.
SEM	Standard error of mean
OLM	Outer limiting membrane.
ONL	Outer nuclear layer.
OPL	Outer plexiform layer.
OS	Outer Segment.
UV	Ultra-violet.
WT	Wilde type.

Glossary

Action Potential	A short term change in the electrical potential that travels along a cell unattenuated in e.g. a nerve.
Apical	Located at, or forming an apex.
Basal	Located at, or forming a base.
Bleached pigment	Pigment that has absorbed a photon and subsequently detached from its opsin.
Brownian motion	Random thermal motion of molecules and particles.
CNG-channel	Cyclic nucleotide-gated channel, also abbr. cGMP-channel.
Distal	Away from the center or other point of reference.
Graded potential	A voltage produced by a neuron which is increasing in amount with incremental stimulation.
Mesopic	The intensity range where both rods and cones are able to operate.
Photopic	The intensity region where only cones operate.
Proximal	Closer towards the center or other point of reference.
Saturated response	Incremental stimulus intensities elicit incremental amplituded responses in the photoreceptors. At a certain point the response amplitude seizes to grow in response to a increasing light intensity, it saturates.
Scotopic	The low-intensity region where rods function, responsible for dark-vision
Second order retinal neurons	Horizontal, bipolar and amacrine cells.
Spatiotemporal	Having to do with both space and time.
Subretinal	The extracellular space between of the outer segment.

Chapter 1

Introduction

Even though vision has been extensively studied, much about its molecular mechanisms remains unknown. The main concepts of vision are thought to be quite known. The part of the eye called retina contains light absorbing receptors (photoreceptors), which convert light into an electrical nerve signal. This conversion of energy from light to electricity is called phototransduction and is mediated by molecular mechanisms in the photoreceptor cells. A single-photon absorption enables the cell to close about 2-5 % [1] of the light-sensitive ion channels. This yields a noticeable potential change over the receptor's cell membrane, which is transmitted through a synaptic connection to subsequent neurons of the visual system. [2]

When subjected to background illumination the photoreceptors have a fantastic capability of regulating their sensitivity. This ability makes it possible for the photoreceptors to reset their "resting" levels and thus successfully detect light over a larger range of intensities than would otherwise be possible. This phenomenon is called light adaptation. The generally known features of light adaptation are acceleration of the photoresponse kinetics as well as a decrease in response amplitude due to the desensitization [3]. Early studies pointed out changes in photoreceptor calcium levels as the reason for adaptation [4]. Today we know that light adaptation is not only regulated by calcium but also has additional regulating mechanisms. Even though the rod photoreceptor (used for night vision) has been extensively studied the full picture of how it adapts to light remains fully unraveled. The light adaptation mechanisms of mammalian cone photoreceptors (used for day vision) have not yet undergone any extensive examination. Many of the molecular mechanisms, though, are thought to be similar to the ones in rods. [5]

There is a great interest in understanding the underlying molecular mechanisms of phototransduction. Understanding why light adaptation functions as it does would shed more light on the process of phototransduction itself. The mouse visual system is of special interest for several reasons. Mice are mammals and therefore their phototransduction mechanisms and genome are very similar to the ones of humans. Moreover the life span of mice is short and they are easy to breed.

At present a large spectrum of ways to genetically manipulate mice is available. [8] Mice have also turned out to be good candidates for disease modeling. The more research can unveil about the normal function of the cellular mechanisms of mice the better the usage of these disease models will be. [8]

The phototransduction electrophysiology can be studied with the electroretinogram (ERG). We record changes over an isolated retina. This means that the light-induced electrical response is a summed signal that originates from many photoreceptors. The advantages of the ERG compared to e.g. the suction pipette method (SP) is firstly, that the mass potential ERG displays an averaged signal from many photoreceptors, while one can only record a photoresponse from a single or a few cells at a time with the SP method. Secondly, the ERG does not cause mechanical stress to the photoreceptors, which is possible in the SP method.

This research program is part of an on-going, larger study focusing on many aspects of light adaptation. This study's main objective was to produce preliminary data for a future study on cone light adaptation. Nikonov et al. paved the way for research on mice cones general electrophysiological characteristics [8]. That study, however, was carried out with the suction pipette method. A later study by Heikkinen *et al.* [9] used the ERG-technique to characterize the mouse cone dark-adapted photoresponses.

The experimental part of this study was conducted in the laboratories of the Department of Biomedical Engineering and Computational Science at Helsinki University of Technology.

The 2:nd chapter of this thesis is an introduction to vision. The eye and its components are presented and the general characteristics of vision are explained. The structure of the retina is presented along with the actual cells that detect light, the photoreceptors. The main focus of the chapter is the molecular signaling cascade of the photoreceptors, which converts the energy of the absorbed photon to electricity.

Chapter 3 deals with the phenomenon of light adaptation and the impact it has on vision. The known mechanisms underlying light adaptation are presented. Furthermore, the known differences between rod and cone light adaptation are discussed.

In chapter 4 the photoresponse, i.e. the electrical response elicited in the photoreceptors by light stimulation, is dealt with in greater depth. The cellular origins of the different components of the photoresponse are presented as well as he different features of the photoresponse. Also, the mass potential ERG that displays the photoresponse is explained.

Chapter 5 describes all the measurement procedures and setups. This includes measurement protocols and analysis methods.

The results of this study are presented in chapter 6. The analyzed data are compared to data found in literature. In the final chapter (7) the reader can find reflections and thoughts on the measurements and how they were done. Some

suggestions on measurement improvements are also included.

Chapter 2

The Vertebrate Eye and Phototransduction

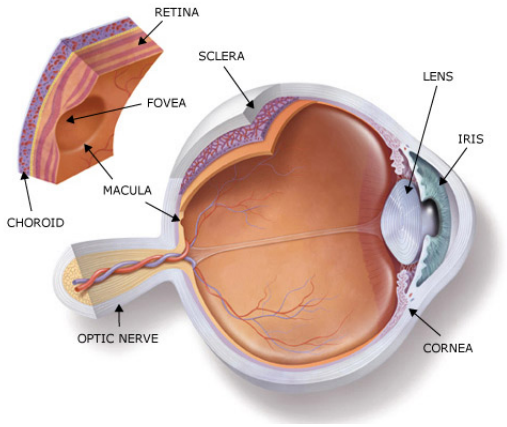

Figure 2.1: The cross-section of a human eye. [12]

2.1 The Vertebrate Eye and Seeing

All vertebrates have a similar eye-structure and way of processing incoming light. The function of the eye is to transport light, convert it into an electrical signal and regulate the amount and quality of visual stimuli that reaches the brain. Light traveling towards the eye first passes the cornea. Thereafter it enters the lens through the pupil. In some species e.g. humans the iris can adjust its size according to the intensity of the light entering the eye. The human lens focuses the light for near or far vision. The light's path continues through the vitreous body, traveling through the proximal layers of the retina without being absorbed. The light absorbing media, the photoreceptors are situated on the posterior side of the retina. [13] Interspecial differences mainly lie in which wavelengths of light different an-

imals are able to detect and discriminate. A cross-section of a human eye and its components is illustrated in figure 2.1. [14]

2.2 The Retina

The retina is made up of several layers (Fig. 2.2). The one closest to the choroid is called the retinal pigment epithelium (RPE) and has the main function of supplying nourishment to the rest of the retina. It contains pigment, which has the function of absorbing stray light [13]. The rest of the retina is made up of layers with different types of neural cells. The first layer, closest to the RPE, holds the photoreceptors. Connected to the photoreceptors' other end are bipolar cells as well as laterally (relative to the other cells in the retina) ranging horizontal cells (Fig. 2.2). The cells are connected via synapses in the outer plexiform layer (OPL). The type of neuronal cell present in the innermost layer of the retina is the ganglion cell. The layer connecting the bipolar cell layer to the ganglion cell layer (GCL) is called the inner plexiform layer (IPL). In the IPL amacrine cells make lateral connections to the axonal side of bipolar cells. The axonal parts of the ganglia exit the retina as a bundle, the optic nerve. No photoreceptors are present where the optic nerve exits the retina and this site is thus called the blind spot. The optic nerve conveys the electrical signal to the parts of the brain that processes seeing, e.g. the visual cortex. Glial cells called Müller cells stretch over almost the entire neural part of the retina (from the ONL to the optic nerve fiber layer (NFL)). Their function is to give the retina structural and metabolic support. No synaptic connections are present between the Müller cells and the other retinal neurons. [27]

2.2.1 Photoreceptors

There are two types of photoreceptors, rods and cones. They are structurally similar in appearance. The outer segment of the rod is cylinder-shaped whilst cones are slightly conically shaped (Fig. 2.3 a and b). The outer segment consists of discs. The difference in disc shape is one of the important differences between the two types of photoreceptors. The circular rod discs, stacked on each other, are disconnected from each other and the photoreceptor membrane. The cone discs, on the other hand, are all attached to each other. The cell membrane has folded itself into discs, which are a part of the cone membrane.

These disc membranes contain the photon-absorbing photopigment, the rhodopsin, as well as many of the proteins associated with the phototransduction cascade. Rhodopsin consists of an opsin part and a retinal part. The opsin is a protein and the retinal is a vitamin A derivative. The retinal undergoes conformational changes, from the bent *11-cis*-retinal to the straight *all-trans*-retinal, when it absorbs a photon. This process is called photoisomerization. When the retinal con-

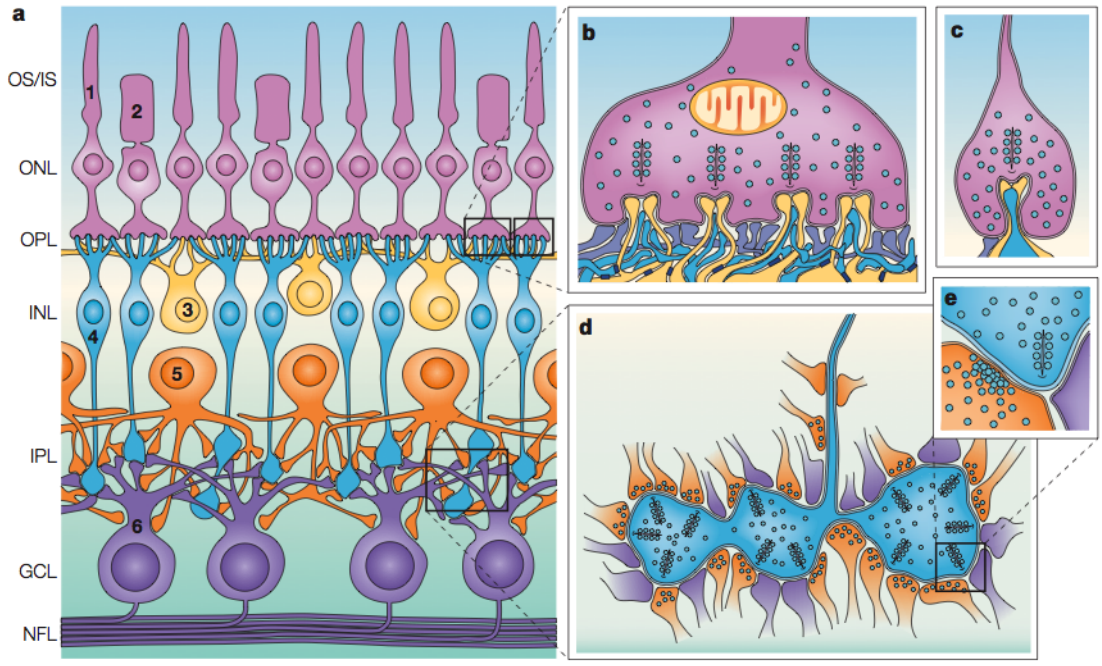

Figure 2.2: **(a)** Structure of the retina. Functionally different neurons make up separate layers. The photoreceptors border to the RPE in the distal part of the retina. The neurons are connected via different types of synapses. **Photoreceptors:** 1. Cone 2. Rod **Second order neurons:** 3. Horizontal cell 4. Bipolar cell 5. Amacrine cell. 6. Ganglion cells. Müller cells are not depicted in this figure. They stretch from the OPL to the NFL (fig. 4.2). **(b)** The cone pedicle and its synaptic terminals. **(c)** The rod spherule, its synaptic terminals. **(d)** A magnified view of the axonal endings of cone bipolar cells (CBC) (blue), and of postsynaptic amacrine cell processes (orange) and rod ganglion dendrites (purple), to which it connects. **(e)** A further magnification of figure d. OS = outer segment, IS = inner segment, ONL = outer nuclear layer, INL = inner nuclear layer, GCL =Ganglion cell layer, NFL = optic nerve fiber layer. [29]

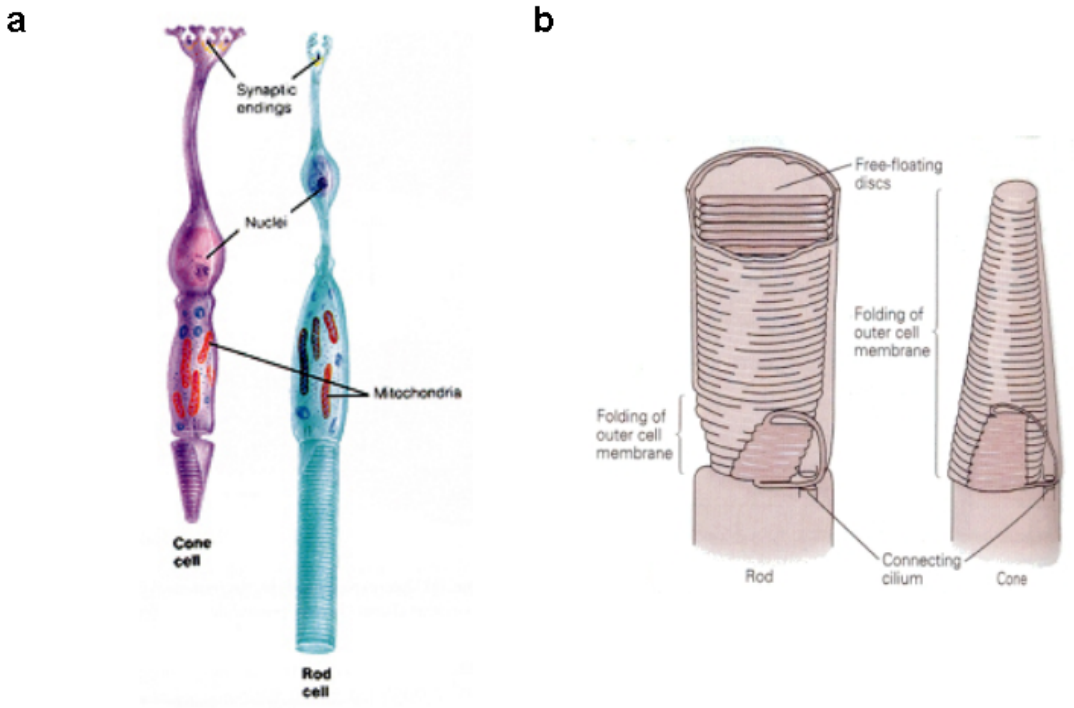

Figure 2.3: **(a)** Structural image of photoreceptor cones and rods. [22] **(a)**The differences in the outer segment of rods and cones. [21]

formation changes the surrounding opsin will consequently change its shape (Fig. 2.4 (b)).

The inner segment comprises the cell's organelles, the nucleus, Golgi complex and many mitochondria [13]. The organelles take care of the cell's metabolism and transport of molecules. At the end of the inner segment both the cone and the rod have synaptic terminals. The terminals have invaginations where the synaptic connections to the second order neurons are made. The rod terminal is called a spherule and only has one invagination while the cone terminal, called a pedicle, has several invaginations (Fig 2.2 b & c). Each invagination can have several bipolar and horizontal cells attached to it synaptically. (Fig. 2.3) [14]

Of the two photoreceptor types rods are the more light sensitive and are used to see dim light. Cones are used for day-vision. Some species with cones have color vision. Mice have three kinds of photoreceportors rods, S-cones, M-cones and UV-cones (S stands for short, M for medium and UV for ultraviolet wavelengths) [16]. The cones-types are categorized by their maximum absorbance wavelengths. Each type of cone has its own type of pigment, which are subsequently called S-,M-, and UV- pigment.

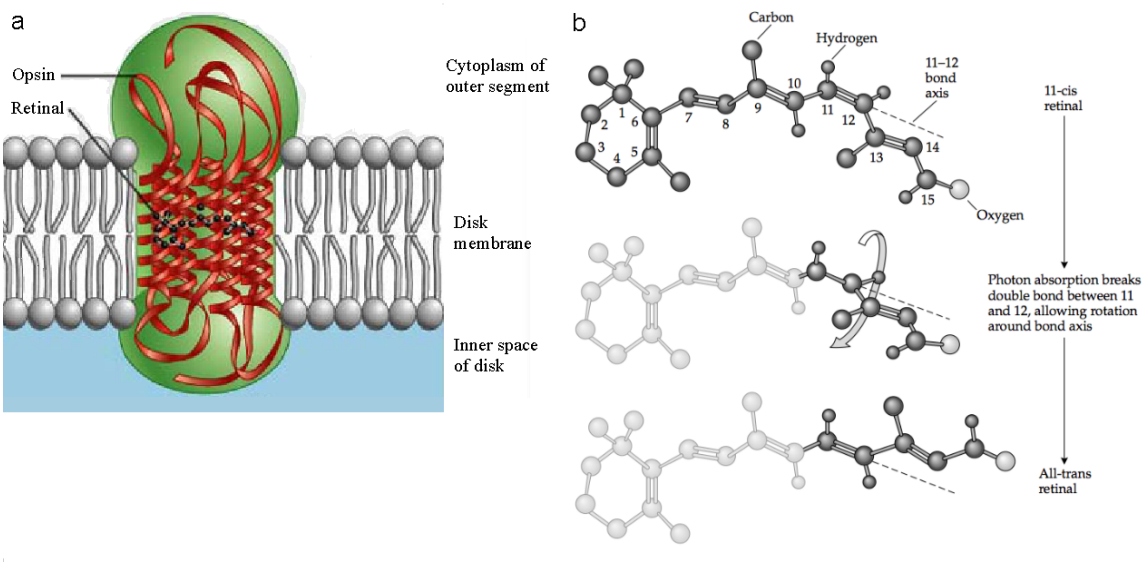

Figure 2.4: **(a)** A rhodopsin molecule as it is anchored in the disc membrane. The opsin consists of an opsin part and a retinal part. [22] **(b)** The absorption of a photon triggers the conformational change of the retinal from *11-cis*-retinal to the *all-trans*-retinal conformation. [1]

2.3 Phototransduction

Once a photon reaches the photopigment in the photoreceptor the pigment may absorb the photon. If the photon is absorbed a cascade of molecules becomes activated. The cascade of activated molecules will cause the cyclic guanosine monophosphate nucleotide gated (CNG) channels in the photoreceptor OS cell membrane to close. Subsequently this will lead to the hyperpolarization of the photoreceptor membrane to a voltage of about -70 mV (Fig. 2.6). The created voltage impedes the release of the neurotransmitter glutamate from the photoreceptors synaptic terminals.

2.3.1 Dark-adapted Transretinal Current

In darkness the photoreceptor membrane potential is about -40 mV, making it significantly more depolarized than most other types of neurons at rest (Fig. 2.5) [15]. In this state there is an inward current of Na^+ and Ca^{2+} through CNG-channels in the photoreceptor outer segment. The outward component of the so-called dark current is balanced by currents through K^+-selective channels in the inner segment of the photoreceptor that transport K^+-ions out of the receptor and the Na^+-Ca^{2+}, K^+ exchangers situated in the outer segment. For every four Na^+ ions transported into the receptor the exchanger moves one Ca^{2+} and K^+ ion out of the cell [20]

To preserve the intracellular Na^+ and K^+ concentrations Na^+ is pumped out and

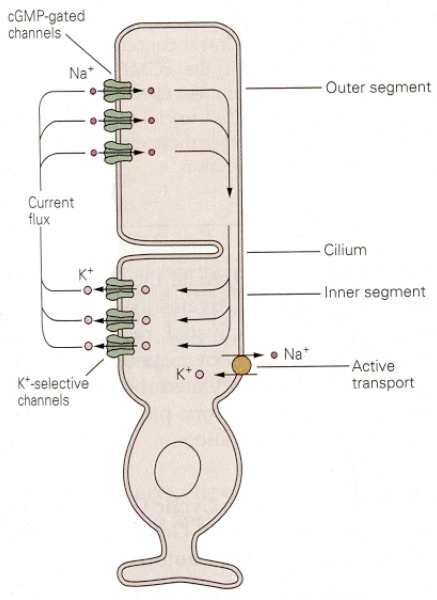

Figure 2.5: The ion fluxes comprising the dark current in a photoreceptor. The inward component consists of Na^+ and Ca^{2+} being transported in by the CNG channels of the OS. Na^+ is also transported in by the Na^+-Ca^{2+}, K^+ exchangers (not depicted in figure) that are situated in the OS. The outward component is made up of an outflow of K^+ through K^+-selective channels. Some of the K^+ does not participate in the radial current through the cell but is transported out already in the OS and Na^+-Ca^{2+}, K^+ exchangers. To keep the ionic concentrations in balance Na^+ is constantly pumped out and K^+ pumped into the receptor by the Na^+/K^+-ATPase. [21]

K^+ is pumped in by Na^+-K^+ pumps [1]. These pumps work against the electrochemical gradient and need adenosine triphosphate (ATP) as their source of energy to function [15].

2.3.2 Activation of Phototransduction

After the absorption of a photon the *11-cis*-retinal in the rhodopsin is straightened out to its *all-trans* conformation, which changes the conformation of the whole photopigment. The now active rhodopsin (R*), in turn, can now bind to and activate the next molecule in the signaling pathway; the membrane bound G-protein transducin (G) (Fig. 2.6).

The transmembrane pigment molecule moves about thermally in the disc membrane and can in its active state activate transducin, which is anchored to the disc membrane (Fig. 2.6). The G-protein consists of three subunits, α, β and γ. The α subunits are bound to GDP. During the activation process the GDP is exchanged for GTP and the now active α-subunit (G*, also called α-transducin) (where the GTP is attached) will dissociate from the $\beta-\gamma$-subunit ($G_{\beta-\gamma}$). [14]

The G* is now able to attach to the γ-subunit of phosphodiesterase (PDE), which is anchored to the disc membrane. The G*-PDE$_\gamma$ complex then dissociates from the rest of the PDE molecule (the α and β subunits). Each PDE molecule has two γ-subunits and they both need to bind to a G* for the PDE α-β-subunit to be fully activated. The function of PDE is to hydrolyze cGMP to guanosine monophosphate (5'-GMP). After transducin attachment the PDE's cGMP hydrolysis rate increases. Consequently the intracellular cGMP concentration is lowered. A fraction of the cGMP-molecules are loosely bound to the cGMP-gated ion channels. As a result of the lowered intracellular cGMP concentration the amount of cGMP bound to these channels decreases. Since a cGMP-gated ion channel is only open when 3-4 cGMP-molecules are bound to it some of them will close. There are tens of thousands of CNG channels in the cellular membrane, and 2-5 % [1] of them will close as a consequence of the absorption of one photon. The ability of one photon to close this many ion-channels is a consequence of the two stages of molecular amplification during the molecule signaling cascade: Firstly, one rhodopsin molecule activates hundreds of transducin α-subunits. Secondly, the PDE* subunits are able to hydrolyze thousands of cGMP molecules during their lifetime. (Fig. 2.7) [1]

2.3.3 Deactivation and Regeneration of Signaling Molecules

The deactivation mechanisms bring the photoreceptor back to the resting state. Every single step in the signaling cascade has its own kinetics and is deactivated in a specific time frame. Notable is that rod and cone photoresponse kinetics are different; cone kinetics are faster.

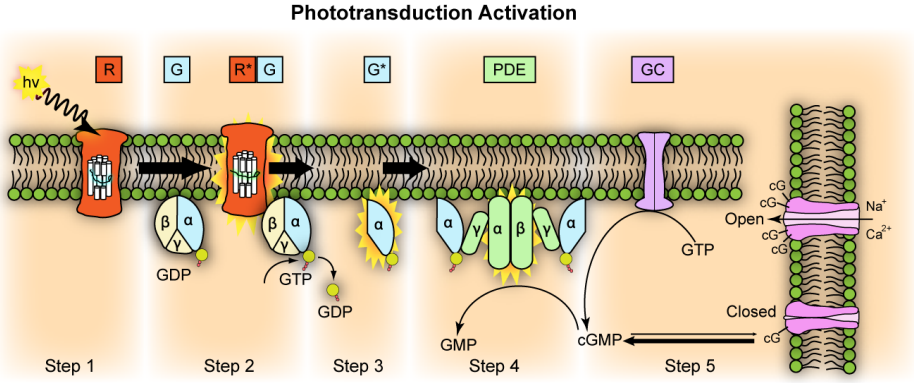

Figure 2.6: The molecule signaling cascade on a rod disc membrane in the OS. **Step 1:** A photon (hν) activates rhodopsin (R*) when absorbed. **Step 2:** R* activates several transducin (G) molecules activating them (G*) as R* moves about the disc membrane. **Step 3:** G* binds to the inhibitory γ-subunit of PDE, when both subunits are bound to G* the PDE is maximally active (PDE*). **Step 4:** PDE* hydrolyzes cGMP into 5'-GMP at a high rate diminishing the free $[\text{cGMP}]_i$ **Step 5:** GC synthesizes 5'-GMP back to cGMP. [23]

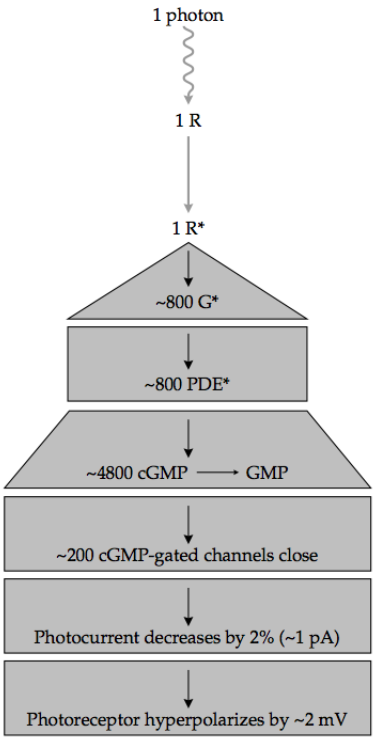

Figure 2.7: The molecule signaling cascade in numbers (monkey rods). The absorption of a single photon can close about 200 CNG (cGMP-gated) channels [1]

The deactivation of R*, a G-protein coupled receptor (GPCR), is performed by several molecular mechanisms, gradually repressing the R*'s catalytic abilities. When R* encounters transducin-molecules in the disc membrane it might also encounter a rhodopsin kinase (RK) molecule. RK is a G-protein-coupled receptor kinase (GRK) that inhibits R* by phosphorylating the part of rhodopin exposed to the cytoplasm [4]. The concentration of RK is about 100 times lower than transducin, so R* will more likely bump into transducin. Furthermore the calcium-dependent protein recoverin (Rec) inhibits the RK-mediated phosphorylation of R* by binding to RK when 2 Ca^{2+} ions are bound to the Rec (Rec-2Ca^{2+} complex). A high $[Ca^{2+}]_i$ results in more Ca^{2+} being bound to recoverin and thereby leaving most of the RK unable to phosphorylate R*. The lowering of $[Ca^{2+}]_i$ caused by a light stimulus will dissociate Ca^{2+} from recoverin in an attempt to compensate for the fall in $Ca[^{2+}]_i$. More RK is now available to deactivate R*. [4]

When R* finally successfully binds to RK the R* will get phosphorylated a number of times, which results in a reduced affinity to bind to G but an increased affinity to bind to the GPCR binding-protein arrestin. Arrestin completely blocks further binding of G to R*. [15] The *all-trans*-retinal then detaches from the opsin (bleaching), which gets dephosphorylated. The retinal is converted back to cis-retinal by retinal isomerase and finally forms a working photopigment by binding to an opsin again (regeneration) [13]. In rods, part of the regeneration process of the retinal is performed in the adjacent pigment epithelium. In cones, the re-

generation of the *11-cis*-retinal is performed not only the pigment epithelium, but also of in the Müller cells. [24]

The G* deactivation takes place when the intrinsic GTPase-accelerating protein (GAP) of G*, called RGS9, hydrolyzes the bound GTP to GDP. The G*'s ability to get hydrolyzed is accelerated by the binding of G_β to RGS9. It has been shown that it is in fact RGS9 that is the rate-limiting factor in deactivation in mice photoreceptor rods [26]. Rate-limiting in this context means that the activity of RGS9 is the slowest of all the deactivation processes and so hinders the photoreceptor from deactivating any faster. It is still unknown if RGS9 is the rate-limiting factor of cones. The fact that the photoresponses recovery is faster in cones and their 100-fold expression of RGS9 [14] might indicate that RGS9 is rate-limiting here as well. [25]

After the light induced closure of the CNG-channels Ca^{2+} influx is severely inhibited. Additionally the 3 Na^+/Ca^{2+}-exchanger keeps transporting Ca^{2+} out of the cell, thereby lowering the $[Ca^{2+}]_i$. GCAPs (Guanylate Cyclase Activating Protein) ability to bind to Ca^{2+} thereby decreases and it looses its 4 Ca^{2+} ions. This enables GCAP to stimulate GC (guanulate cyclase), which accelerates its cGMP synthesis. This will accelerate the return of $[cGMP]_i$ to reach its resting levels. [15]

Chapter 3

Light Adaptation

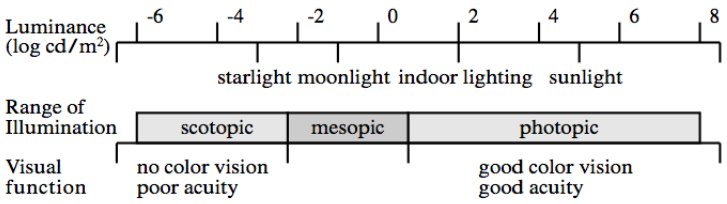

Figure 3.1: The top picture presents the intensity spectrum that the visual system encounters in nature in Cd/m^2. In the bottom picture the respective intensity ranges where the photoreceptors function; the lowest intensity-range, where rods function, is called scotopic; the higher intensity-range, where solely cones operate is named the photopic. The region in-between, where both photoreceptors function, is called mesopic. [44]

The visual system is subjected to a wide spectrum of light intensities (Fig. 3.1). To be able to function over this whole range the visual system has developed methods of adjusting to changing background lighting. At the photoreceptor level, the cells become less sensitive to incoming light, as the background lighting gets stronger. The rods are responsible for the first 3-4 decades of illumination the eye is able to detect. When entering the photopic range of light intensity cones are able to signal the absorption of a photon, while rods saturate unable to signal the detection of any photons further. The cones can adapt in the remainder of the intensity-range and virtually never saturate when subjected to incremental light intensities.

The majority of the known facts on light adaptation are based on studies on rods. Most phenomena associated with light adaptation are assumed to be similar in cones. However, some mechanisms are known to be different in cones. These are discussed in section 3.3.

Background illumination causes changes in the photoreceptor electrophysiology. A light-adapted photoresponse is thus generally faster compared to dark-adapted ones. Also, the desensitization of the photoreceptors will cause the photoresponse amplitude to decrease (when subjected to a stimulus of the same magnitude). The

sensitivity of photoreceptors has been found to follow Weber's law (at least rods) (Fig. 3.2). Weber's law states that the photoreceptors's flash sensitivity S_F is:

$$\frac{S_F}{S_D} = \frac{I_B}{I_B + I_0}, \tag{3.1}$$

where S_D is the sensitivity in darkness, I_B is the background intensity and I_0 the intensity needed to halve the sensitivity.

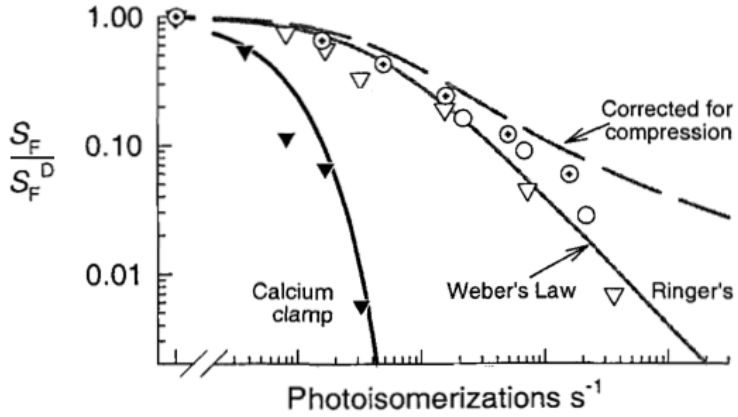

Figure 3.2: The sensitivity normalized with the sensitivity in darkness as a function of background intensity. Open symbols represent measurements made in Ringer's solution (three different retinas) (fitted to Weber's law (light grey line)). The black triangles represent the calcium clamped case. [4]

If calcium is held at dark-adapted levels (clamped) the cell looses some of its ability to perform this intensity range extension (Fig. 3.2 Black triangles). When applying increasingly stronger background intensities the drop in sensitivity is far greater than in vivo circumstances. A decrease in $[Ca^{2+}]_i$ therefore does not cause desensitization, but rather rescues the cell from a too rapid desensitization and subsequently extends the operational intensity-range.

Temporally light adaptation can be categorized into fast and slow mechanisms. Fast mechanisms act upon the photoreceptors instantaneously and slow over a period of seconds to minutes. The main calcium dependent mechanism is GC activity-regulation by Ca^{2+} [3] and the main non-calcium dependent mechanism results from an increase of active PDE [4]. The other adaptational mechanisms are: Response compression, other Ca^{2+}-regulation mechanisms, pigment bleaching, and protein translocation.

3.1 Calcium Dependent Mechanisms of Light Adaptation

Light induced closing of the CNG-channels causes the flow of calcium into the photoreceptors to decrease and with that the $[Ca^{2+}]_i$ will fall. This regulation of the calcium-level in turn affects several phototransduction mechanisms linked to visual adaptation. Regulation of PDE and GC activity as well as channel affinity are three of the known mechanisms. [5]

3.1.1 Regulation of Guanylate Cyclase Activity

The GC activity is sped up by the fall in the $[Ca^{2+}]_i$. GC activity causes the rate of cGMP synthesis to increase. This balances up the light induced fall in cGMP concentration. In steady background illumination the steady-state $[cGMP]_i$ is therefore lowered compared to dark conditions resulting in a higher occupation of the cGMP binding sites on the CNG-channels keeping a larger number of them open. The complete closure (to a certain point) of all the CNG-channels is thereby prevented and the photoreceptors are rescued from saturation. The photoreceptor sensitivity is increased in comparison to what it would be in the absence of this mechanism.

GC also affects light adaptation transiently as a response to a flash of light. After a flash of light $[Ca^{2+}]_i$ decreases transiently causing a transient increase in the GC activity. Here the recovery of the flash responses is sped up and the amplitude is decreased compared to the case that GC activity would not be accelerated (desensitization). [4]

3.1.2 Regulation of CNG-Channel Affinity

CNG-channels affinity to bind cyclic GMP depends on $[Ca^{2+}]_i$. When the concentration of calcium decreases Ca^{2+}-cations are released from calmodulin, which now detaches from the β-subunits of the CNG-channels (Fig. 3.3). The CNG-channels affinity for cGMP to dock on them thereby increases leaving more of them open. The concentration of cGMP needed for half-maximal opening of the CNG-channels, K_{cG}, gets shifted upwards. K_{cG} of cones CNG channels, on the other hand, seems to have another modulator than calmodulin, a not yet identified molecule. The effect is prominent over the cones whole physiological range. [4] In rods the effect is not that prominent.

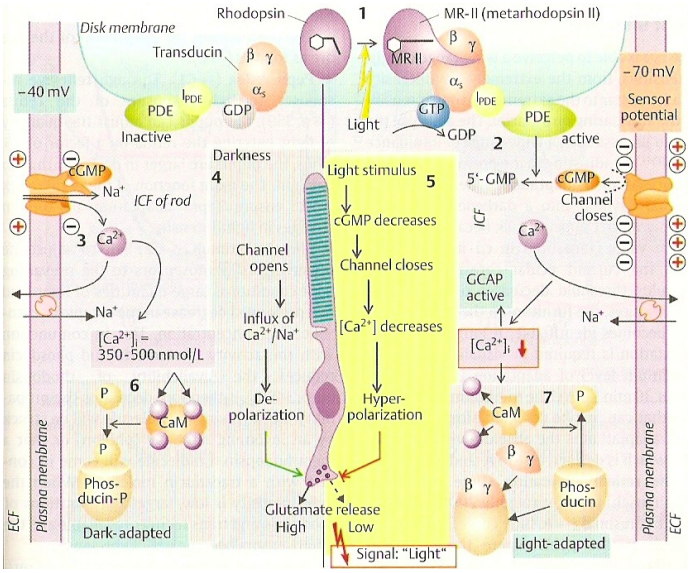

Figure 3.3: Calcium changes that contribute to light adaptation. [15]

3.1.3 Calcium Buffering

The photoreceptor opposes the drop in $[Ca^{2+}]_i$ by buffering calcium. Because GC activity is triggered by this decrease its onset becomes somewhat delayed. Consequently the activation of cGMP synthesis is also delayed and more CNG-channels have time to close before GC can start to balance up the light-induced breakdown of cGMP. The photoresponse amplitude increases and the deactivation time is prolonged. Recoverin is thought to be the main calcium-buffer in rods, i.e. when $[Ca^{2+}]_i$ decreases due to a light stimulus more recoverin will release the calcium bound to it trying to maintain the original $[Ca^{2+}]_i$. With this buffering the relative sensitivity of the photoreceptor increases. [4]

3.1.4 Regulation of PDE-activity

The $[Ca^{2+}]_i$ also regulates the activity of PDE. However, the effect is only evident when the level of intracellular calcium has been lowered considerably. A large reduction in $[Ca^{2+}]_i$ is possible by either a long-lasting or very bright flash-stimulus. The suggested mechanisms for the regulation of the PDE activity: A recoverin $2Ca^{2+}$ complex inhibits RK from phosphorylating R*, which would start the deactivation of R*. The light-induced fall in $[Ca^{2+}]_i$ will cause the recoverin-bound calcium to dissociate. More RK is now available for R*-deactivation. [46]

3.2 Light Adaptation Mechanisms Independent of Calcium

3.2.1 Response Compression

Continuous illumination leaves fewer CNG-channels open and the steady-state circulating current of the photoreceptors is reduced compared to darkness. Fewer channels are now open to be modulated by additional flashes of light. Compression is not actually light adaptation but rather an inevitable consequence of phototransduction. Comparing responses with each other will therefore include this non-adaptive component. If the response is normalized in respect to the maximum response the fractional change caused by the test flash can be seen. [4] [45]

3.2.2 Steady-state PDE-activity

The amount of free intracellular cGMP depends on the rates of hydrolysis and synthesis of cGMP. Since light stimulates the activity of PDE the amount of active PDE in steady illumination will be higher compared to the dark state. The relative change in cGMP concentration is dependent on the overall activity of PDE. A photon will therefore cause a relatively large response in darkness. The changes in $[\text{cGMP}]_i$ are now relatively large. In a light-adapted state the relative decrease in $[\text{cGMP}]_i$ will be smaller and the resulting electrical response will be smaller. Due to the accelerated hydrolysis and synthesizing rates the cGMP-level is brought back to the steady state level much faster. This causes the response to accelerate. At present this mechanisms is believed to contribute the most to light adaptation.[4], [46]

3.2.3 Protein Translocation

One of the newest discoveries concerning light adaptation is protein translocation. In bright light certain proteins are translocated between the rod outer segment (ROS) and the rod inner segment (RIS). In darkness most of the α-transducin and recoverin [46] is located in the ROS. Arrestin is mainly located in the RIS. Bright light causes the arrestin to start moving to the ROS and α-transducin to start moving to the RIS. This translocation is thought to contribute to light adaptation. [40, 46]

3.3 Light Adaptation in Cones

The basic mechanisms of rod and cone phototransduction and light adaptation are the same. The light induced fall in free $[\text{Ca}^{2+}]_i$ is faster in cones compared to rods.

The Ca^{2+}-feedback mechanisms might hence become activated faster as well as being more forceful in cones [46]. This might contribute to differences in light adaptation (as well as phototransduction). Also, the biochemical function and transduction molecule concentration might also contribute to differences in the rod and cone light adaptation kinetics described in the previous section. Protein translocation has also been shown to function differently in rods and cones. An additional light adaptation mechanism in cones is pigment bleaching. In rods the effect of pigment bleaching does not become apparent before the rod saturates.

3.3.1 Pigment Bleaching

Pigment bleaching only has a marginal contribution in normal lighting conditions. Only at very high illumination does pigment bleaching have a more prominent impact on light adaptation of cones.

After a pigment has absorbed a photon the retinal experiences a re-conformation (the retinal transforms from the *11-cis*-retinal to the *all-trans*-retinal). The re-confromation subsequently leads to a detachment of the retinal from the opsin and this process is called pigment bleaching. Pigment bleaching is substantial when the retina is subjected to bright lights. Less pigment is therefore available for absorption. The retina is subsequently desensitized. [5, 46]

3.3.2 Protein Translocation

In mice, protein translocation has been shown to function differently in cones compared to rods (Rod protein translocation, section 3.2.3). In darkness the cone α-transducin is located in the cone outer segment (COS). In contrast to rods, the cone α-transducin has not yet been seen to translocate at all in response to the light intensities available. Arrestin is located in the cone inner segment (CIS) during dark-adapted conditions and translocates to the COS in response to bright light. [40]. The functional consequences of protein translocation have not yet been fully elucidated. [46] It has been hypothesized that translocation could be involved in light adaptation and/or protection against light damage of the photoreceptors. [40]

Chapter 4

Photoresponses and the Electroretinogram

Photostimulation causes the radially flowing ion currents (transretinal current, Fig. 2.5) in the interstices of the retina to change.

The changes in the transretinal currents can be indirectly recorded with various techniques (i.e. the current from all the retinal cells are recorded simultaneously) by measuring the voltage generated over the retina. Today the ERG-technique is used both in clinical diagnostics and vision research.

Clinically the method is always non-invasive. A contact lens with an $Ag/AgCl^{-}$-electrode is placed on the surface of the cornea and a reference electrode on the forehead, temple or earlobe. In research laboratory settings methods that record responses straight from an isolated retina or from the cup of the eye are also used. To measure the transretinal potential in isolated retina electrodes are placed on top and on the bottom of the retina. In this study ERG-recordings are done on isolated mouse retinae.

4.1 The Components of the Photoresponse

To understand the molecular processes that compose the ERG one can try to separate its components. This can be done in several ways. In the early work of Ragnar Granit in 1933 he separated the PI, PII and PIII components by studying anesthetized cats. These components were named after how fast the components disappear after applied anesthesia [28]. At this time the origin of the ERG components were unknown. Another way of categorizing the ERG components is by splitting up the ERG in an a-, b-, and c-wave. In bright light some animals also produce an additional nose component [33]. They are shown in figure 4.1 with the complement of the PI, PII and PIII-components, which will yield the complete ERG upon superpositioning. [27] The ERG-signal is composed of a sum of responses from several retinal components. Since it is a summed signal from all the

photoexcited photoreceptors and second order neurons in the retina only parts of each component can be distinguished. A flash response ERG-signal is shown in figure 4.2 including which cell or process that generated each component. Table 4.1 is a summary of the origin of these potentials.

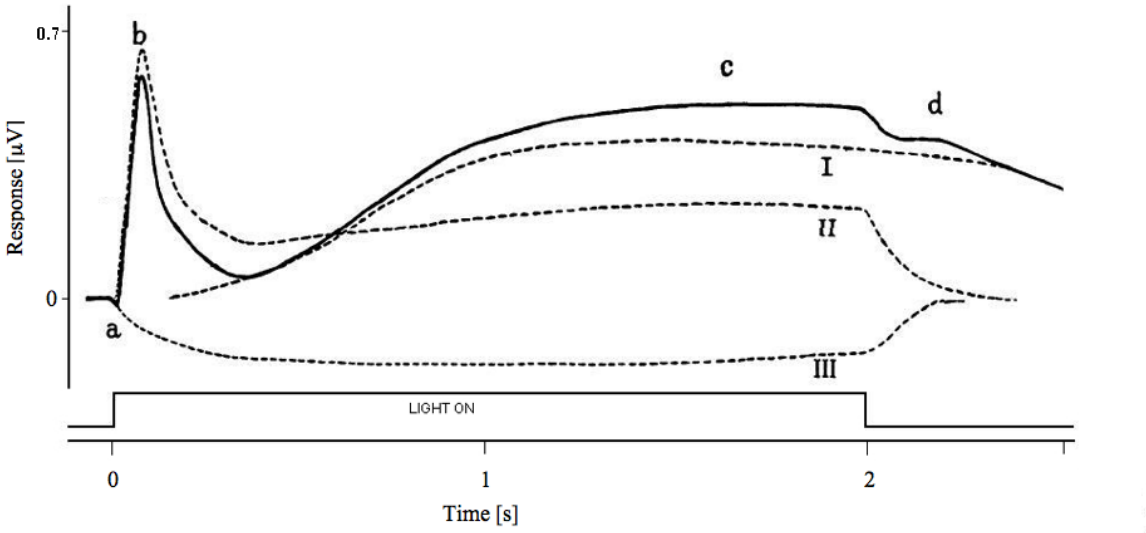

Figure 4.1: The electroretinogram of the vertebrate retina as depicted by Ragnar Granit. The dashed lines representing the separated PI(I), PII (II), and PIII (III) components. The black line shows the superimposed ERG and the location of the a,b and c-wave. [28] (Modified)

Table 4.1: The components of the ERG [28]

R_1 and R_2	The initial changes in the photopigments, caused by light action, also called early receptor potential (ERP).
a–wave	The actual response from the photoreceptors.
Oscillating potentials	Caused by second order retinal neurons, horizontal and bipolar cells. Appear in the light-adapted b–wave.
b–wave	ON–bipolar cell activity.
c–wave	Generated by the retinal pigment epithelium.
n–wave	Early negative overshoot component of the a-wave, appear in some animals.

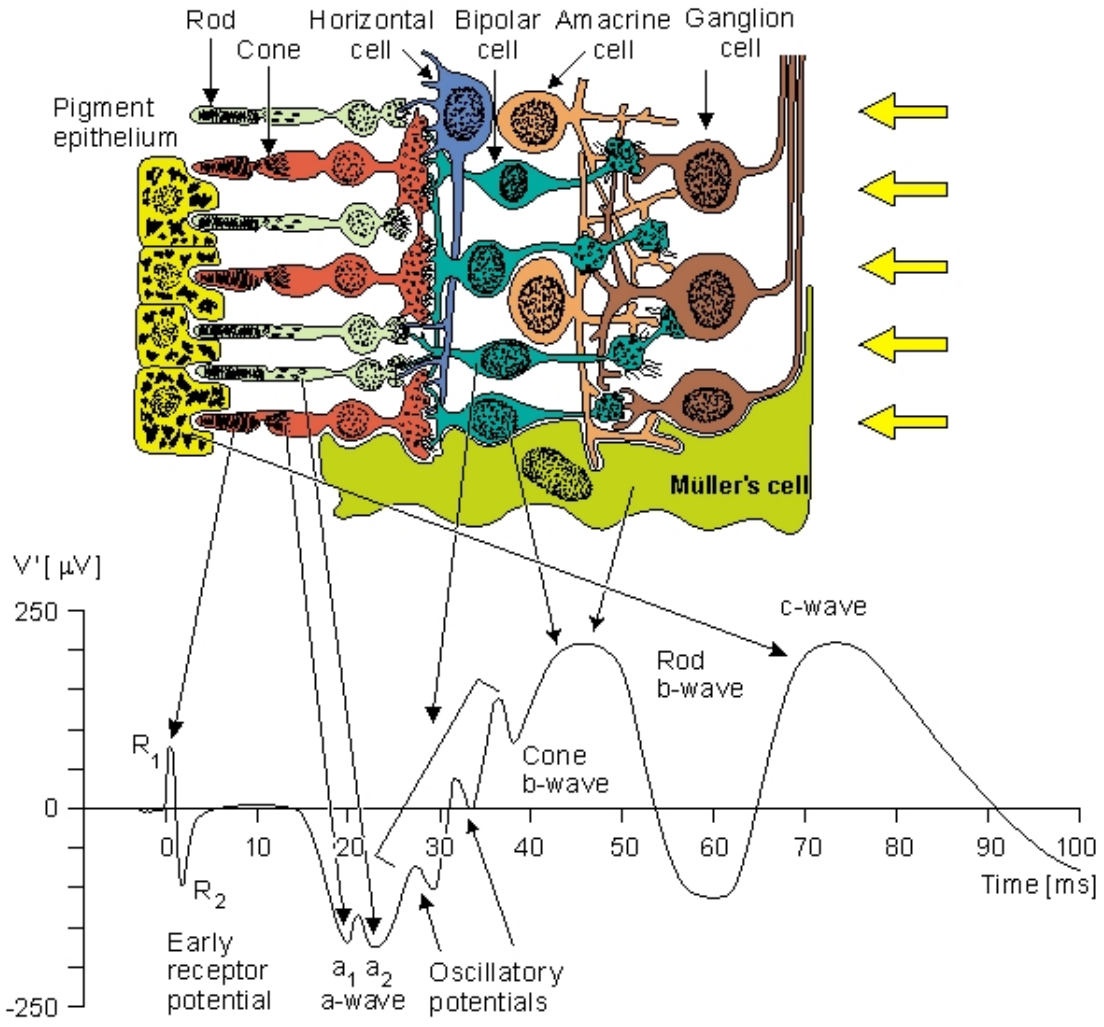

Figure 4.2: The electroretinogram of the human retina. The cellular origins of the ERG-curve are shown. [27]

4.1.1 The a-wave and fast PIII component

The electrophysiological activity of the photoreceptors themselves gives rise to the a-wave. It is visible only briefly in the beginning of the fast PIII component. Thereafter the electrical activity of the photoreceptors is overshadowed by the activity of other retinal cells. The beginning part of the PIII component is called the early receptor potential (ERP) (Table 4.2), and only appears when the retina of some species is subjected to a short high intensity flash. The intermediate part of the PIII is the response from the photoreceptors (from rods and cones). The remainder of the PIII (slow part) component arises from Müller cells and is described in section 4.1.4.

The mechanisms of the a-wave are: When a photoreceptor is stimulated the radially circulating current subsequently decreases. This translates into a drop in voltage seen across the retina.

4.1.2 The b-wave

The b-wave originates from ON bipolar cell activity caused by light stimulation. The hyperpolarization of the photoreceptor release of the neurotransmitter glutamate to decrease. Receptor in the bipolar cell membrane sense the decrease in glutamate release and respond by opening some of its cation channels, through which cations flow into the bipolar cell. To compensate for this influx of cations ion channels in the proximal part of the bipolar cells transport the cations out of the cell (Fig. 4.3). [31, 32]

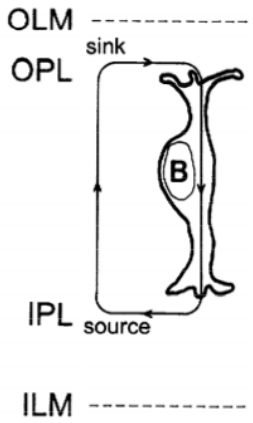

Figure 4.3: The currents that give rise to the b-wave. [31]

4.1.3 The c-wave

The pigment epithelial cells give rise to the c-wave. As a response to photostimulation the $[K^+]_o$ decreases in the proximity of the pigment epithelium. The lowering of $[K^+]_o$ causes the apical retinal pigment epithelium (RPE) to hyperpolarize. This, in turn, catalyzes the basal part of the pigment epithelium to subsequently hyperpolarize. The c-wave, or PI, is therefore a measure of the transepithelial voltage, that is the voltage over the whole RPE. [42]. The resting K_o^+-level is then reestablished with K^+ that enter the subretinal space from the REP through K^+ rectifier channels in the apical membrane. [43].

4.1.4 The Slow PIII

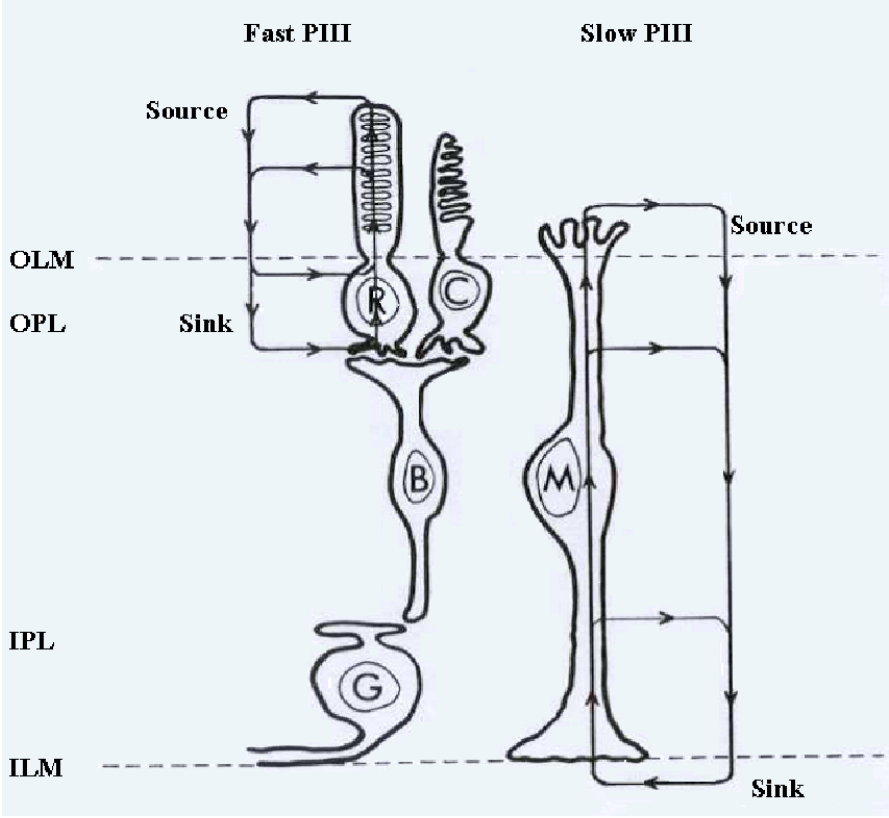

Figure 4.4: The current flow of K^+ that gives rise to the fast and slow PIII components. The fast component originates in the photoreceptors and has its source in the photoreceptors outer segments while the sink lies in the inner segment of the receptors. The source of the slow PIII is situated in the distal part of the Müller cells and has its sink at the Müller cells end feet. [30]

The slow PIII component is caused by the Müller cells. The subretinal $[K^+]$ is lowered in response to photostimulation because the photoreceptor inner segments now transport less of the cations out of the cell. The adjacent distal parts of the

Müller cells then release K^+ at the proximal parts of the subretinal space. The efflux of K^+ at the Müller cells distal part (current source) is replenished with K^+-ions from the cells proximal parts (flowing intracellularly). Now an extracellular current flows from the source to the proximal part of the Müller cells (sink). The extracellular current-flow generates a voltage that can be seen as the slow PIII component of the ERG. (Fig. 4.4) [30]

4.1.5 The Nose Component

Some mammals display an additional a-wave component, the nose component. However, it will only manifest itself in nearly saturated and saturated responses. The study of the nose component origins has been started quite recently and the exact origin has not yet been determined with certainty. However, the following description describes the current hypothesis. [33]

The nose component is thought to be generated by an own current loop formed in the inner segment of the photoreceptors. The current loop is constructed of a current through h and K_x channels. In darkness the majority of the h channels are closed and most of the K_x channels are in an open state. A weak flash of light will not change the membrane potential enough to alter the state of any of these channels. Subsequently no change in the current is created. A saturated light flash causes the membrane potential to hyperpolarize substantially opening a significant number of h channels. When the following hyperpolarization gets large enough the current going through the K channels will decrease, which is caused by both the a diminution of the driving force and the voltage-dependent closure of the K_x channels. [33]

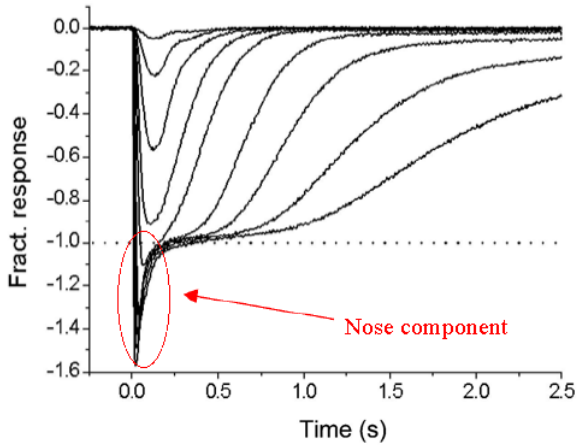

Figure 4.5: The nose component in a mouse rod ERG. [9] (Modified)

Chapter 5

Methods

5.1 Preparations and Solutions

In this study pigmented mice (C57B1/6) were used. Additionally a genetically modified mouse was tested. α-transducin knockout mice lack functioning rods, i.e. these mice have rods but these do not respond to light. The functioning of the rods is disabled by the deletion of the rod α-transducin gene. The result should be is a mouse that has only functioning cones. [34]

The mice were handled and cared for in accordance with Finland Animal Welfare act of 1986 and the guidelines of the Animal Experimentation Committee of the University of Helsinki.

The mice were dark-adapted over a minimum period of 3 h, but usually overnight. The measurements were made on isolated retinae. Firstly, the mice were anaesthetized with CO_2 and then killed. Then the eyes were enucleated and bisected along the equator to open the eye up and remove the retina. The dissection procedure was done in cooled Ringer's solution under a dim red light in a dark-room.

5.1.1 Solutions

The retinae were perfused with Ringer's solution (Table 5.1) until stabilization. Leibovitz culture medium L-15 was administered to better the retina's viability. In the first experiment the pH was set to 7.5, but in order to improve the stability of the retina the pH was raised to 7.8.

5.1.2 The ERG-apparatus

The ERG-apparatus (Fig. 5.1) consists of lasers that act as light-sources, a set of mirrors, lenses and beam splitters that lead the laser beams to the light guide, which transport the light to the retina. The magnetic shutters placed in front of

Table 5.1: Ion concentration of the Ringer's solution

	Concentration [mM]
NaCl	133.0
KCl	3.3
$MgCl_2 \cdot 6H_20$	2.0
$CaCl_2 \cdot 2H_2O$	1.0
D-glucose	10.0
EDTA	0.010
HEPES	12.0
Na-aspartate	2.0
NaOH	5.8

the lasers were used to control the duration of the light stimulus. The lasers used in this study were a 543.5 nm HeNe laser and a 532 nm HeNe laser (green light), both lasers being of the brand Melles Griot. The light intensity was regulated with calibrated neutral gray filters and wedges. The light intensity was regularly measured with a calibrated photo diode.

The retina was positioned on a specimen holder with its proximal side down. Ringer's solution was perfused over the distal part of the retina. The perfusion rate was $\tilde{2}$.8ml/h. The proximal side of the retina (laying against the specimen holder) was coupled to a chloride solution containing 10 mM BaCl through a porous Millipore paper (Fig. 5.2). The specimen holder was located on heat exchanger that has temperature-controlled liquid flowing through it. Thereby the retina can be cooled down or heated up to the desired temperature by an external cooler. A thermistor in the specimen holder was used to measure the retinal temperature. The transretinal potential was measured with $Ag/AgCl^{-}$ pellet electrodes placed on both sides of the retina.

The specimen holder was placed in a Faraday's cage in order to isolate it from the electrical disturbances. The Ringer's solution as well as all other equipment that possibly could induce electrical disturbances in the ERG-signal are coupled to the signal earth. The Ringer's solution was also isolated from electrical disturbances.

The ERG signal was first amplified by a factor of 100 by a differential amplifier. Then the signal is further amplified 10 times in another amplifier. The signal was then low pass filtered with a minimum cut-off frequency of 1000 Hz. A data acquisition card (National Instruments) collected the signal with a collecting frequency of 2000 Hz and converted it to digital form.

The stimulus protocols were controlled through the same data acquisition board controlled by a software especially designed for this purpose.

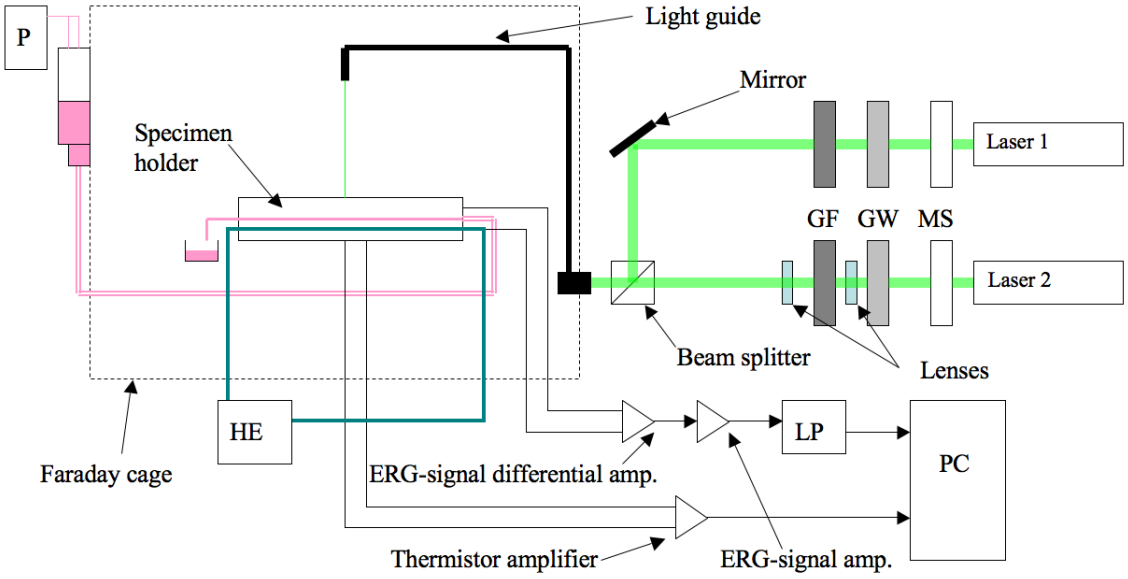

Figure 5.1: The setup of the ERG apparatus used in this study. The light reaching the retina is attenuated by the GW (gray wedge) and GF (gray filter). To give the laser beam from laser 2, an appropriate diameter for the light guide two lenses adjust the size of it. The beam splitter joins the two beams together. The specimen holder (Fig. 5.2) is placed on heat exchanger (HE, metal plate). The ERG-signal and the signal from the thermistor are amplified by differential amplifiers. The ERG-signal is further amplified in an additional amplifier (not differential). The ERG signal is then low-pass filtered. Peristaltic pump (P) was used to drive the Ringer's solution.

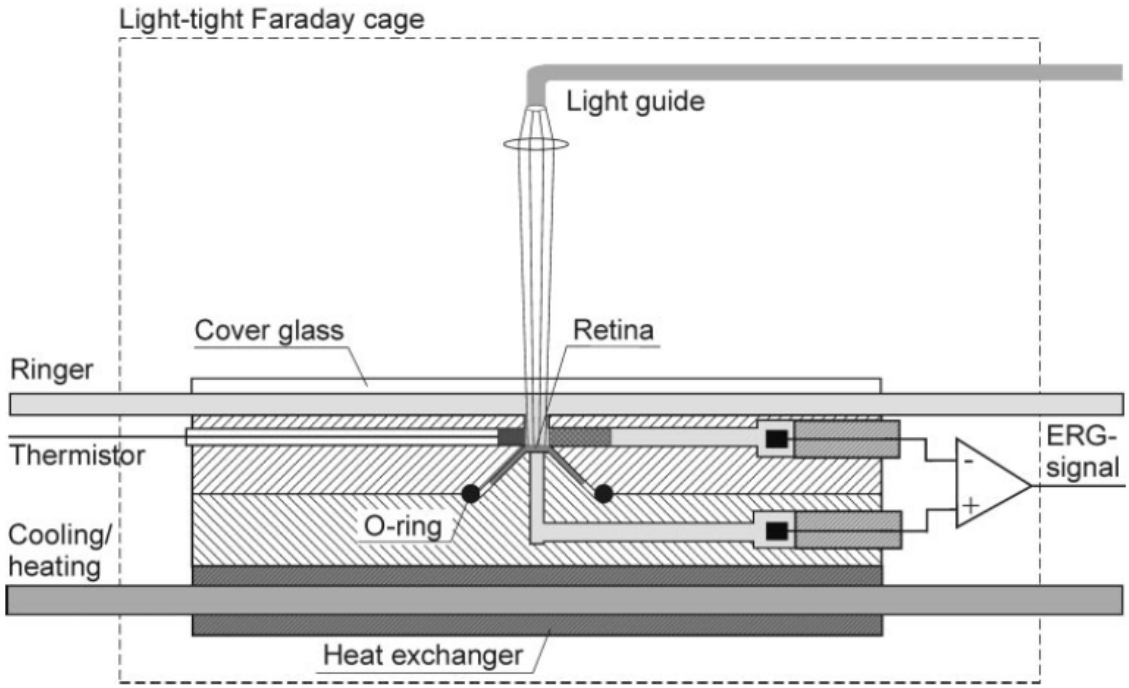

Figure 5.2: The ERG specimen holder (SH). The retina rests on the lower part of the SH and Ringer's solution is superfused on the retina through the upper part of the SH. Ag/AgCl^{-} electrodes in the upper and lower part of the SH measure the voltage over the retina. The temperation of SH was controlled by a heat exchanger that the SH is placed on. The Ringer's solution is heated to the same temperature by also flowing through the same plate. The temperature is measured by a thermistor placed in the SH near the retina. [41]

5.1.3 Determining the Stimulus Intensities and the Number of R* produced in Rods

To determine the stimulus intensity in photons per second and unit area the following steps are taken: The intensity of the light source is I_0. It is then attenuated with a total optical density of D. The intensity (I_F) of the beam after passing through the filters is:

$$I_F = I_0 \cdot 10^{-D} \tag{5.1}$$

The axial end-on collecting area a_c of the rod, which is the effective area that absorbs photons, can be calculated in the following manner:

$$a_c = f\frac{\pi d_{rod}^2}{4}\left[1 - 10^{-\Delta D(\lambda)\cdot l_{rod}}\right]\gamma, \tag{5.2}$$

where f is a dimensionless factor that accounts for the light funneling by the photoreceptor inner segments. In our recordings the light enters the retina from the epithelial side and light funneling is negligible, i.e. $f = 1$. d_{rod} and l_{rod} are the diameter and the length of the outer segments respectively. $D(\lambda)$ expresses the specific optical density of the outer segment at the wavelength λ, $l_{rod} = 24\mu$m is the length of the rod outers segments. γ is the photoisomerization quantum efficiency and is $\lambda_{max}\ \frac{2}{3}$. The number of R* per photoreceptor cell is determined by multiplying I_F with the a_c.
Eq. 5.3 determines the specific absorbance of photons at the stimulus wavelength used:

$$\Delta D(\lambda) = x(\lambda) \cdot D(\lambda_{max}), \tag{5.3}$$

$D(\lambda_{max})$ is the greatest absorbance for a specific type of photoreceptor (here rods), i.e. the amount of absorbed photons depend on the wavelength of the light and also on the type of photoreceptor that the light encounters. $x(\lambda_{max})$ is the fraction of $D(\lambda_{max})$ at a certain wavelength.

The number of photons (stimulus intensity I_F) absorbed by photopigments in a single rod with a_c is then:

$$\Phi = I_F \cdot a_c \tag{5.4}$$

5.1.4 Determining of the Number of R* Produced in Cones

Determining the number of photoisomerizations in the mouse cone for certain intensities and wavelengths is not as simple as with rods. Firstly, the pigment in M-cones is not exclusively of M-pigment. Secondly, the rod outer segments might shadow the COS.

The size and shape of cones are somewhat different from rods. The mouse cone shape is slightly cone-shaped but can be estimated as a cylinder. Using approximation and equation 5.2, we get, $a_{c,cone} = 0.29\mu$m (the COS dimensions $l = 1.2\mu$m and $d = 13.4\mu$m.)

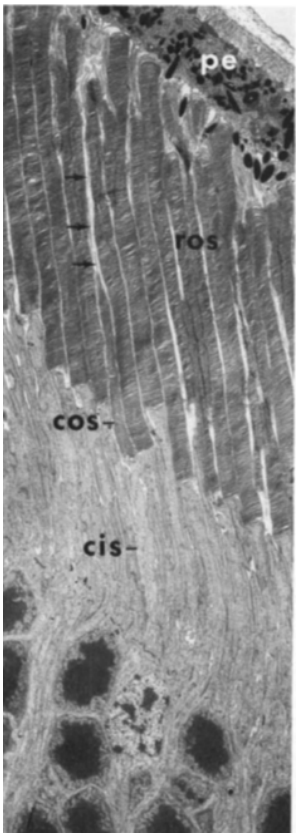

Figure 5.3: Position of rod and cone outer segments (ROS COS). The ROS are roughly twice as long as COS, which are connected to the pigment epithelium (PE) via long villous pigment epithelial cell processes (arrows). The ROS are in contact with the PE close to the somata of PE cells. [6]

The rods are estimated to shadow cones by half of the length of their outer segments (Fig. 5.3). When the shadowing of the rods are taken into account, the corrective term derived is:

$$k_{shadow} = 10^{-D(\lambda)\cdot\frac{1}{2}\cdot l_{rod}}, \tag{5.5}$$

where $D(\lambda)$ is the rod optical density.

Furthermore, in mice cones there is some co-expression of opsins. Seemingly there are two main types of cones containing the M-opsin, one where S-opsins are predominating, another with a more equal amount of S and M opsin. It is still unknown exactly how S and M cones are distributed on the mouse retina including the distribution of opsins in the different photoreceptors themselves. The actual

fraction of M opsins available on the recording area has been calculated to be 35% on average [9].

Since the S-pigment response to the wavelengths used in this study (543.5 nm and 532) it was deemed as unresponsive. Left to absorb photons are then the 35 % of the total amount of pigments (S and M pigments), that on average reside in the cone photoreceptors of a mouse central retina. The optical density of the retina is therefore further modified to the value $\Delta D_{mod}(\lambda)$ (Eq. 5.6). [9]

$$\Delta D_{mod}(\lambda) = 0.35 \cdot \Delta D(\lambda) \tag{5.6}$$

The collecting area for a cone finally becomes:

$$a_c = f\frac{\pi d_{cone}^2}{4}\left[1 - 10^{-\Delta D_{mod}(\lambda)\cdot l_{cone}}\right]\gamma \cdot k_{shadow} \tag{5.7}$$

The actual intensity that absorbed by the retina is again calculated with equation 5.7.

5.2 The Photoresponses

5.2.1 Isolation of the Photoreceptor Component

In this study the interest lies in studying the flash responses of the photoreceptors. If the total ERG-signal from the retina were to be recorded the photoreceptor component would be buried in the (total) ERG signal. Therefore the fast PIII, the component of interest, has to be separated from the rest of the ERG. It can be extracted from the ERG-signal by adding aspartate, which will block the glutamate receptors on the bipolar cells [2]. Now, the bipolar cells cannot detect changes in glutamate release by the photoreceptors and their function is disabled.

The slow PIII, caused by the Müller cells, is neither of interest in these measurements. It is also eliminated from the ERG-signal pharmacologically. Barium blocks K^+-channels. Here it is applied to the proximal side of the retina to only block the Müller cell end feet K^+-channels and not the cation channels of the photoreceptors. This cuts off the K^+ flux of the Müller cells.

The c-wave does not appear on the ERG of an isolated retina since its origin, the pigment epithelial cells are separated from the retina during dissection. The result of this yield an ERG that can be viewed in figures 5.4 (a) (rods) and 5.4 (b) (cones).

5.2.2 Separation the Rod and Cone Responses

When performing measurements in the mesopic intensity region responses are elicited from both rods and cones. The separation of the cone signal is performed

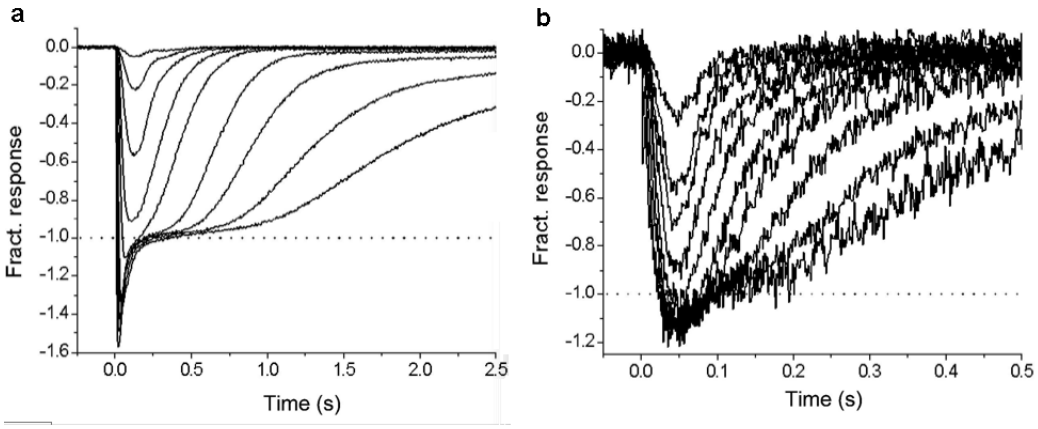

Figure 5.4: **(a)** The electroretinograms of a fractional rod response family. **(b)** The electroretinograms of a fractional cone response family. [9]

in the following manner: Steps of background light were given to saturate the rod photoreceptors. Then an additional flash is given during rod saturation. Since rods cannot respond at this time the additional flash can only elicit a response from cones (Fig. 5.5 magenta curve).

To ease the separation of the pure cone response from the (not always that constant) rod saturation level, a substraction method was used. Rod-saturating photoresponses were first recorded without the test-flash that elicits the cone response (Fig. 5.5 purple curve). Then a rod-saturating response is recorded with a cone response. The former (Fig. 5.5 magenta curve) photoresponse is subtracted from the latter resulting in a photoresponse that originates solely from cones (Fig. 5.5).

5.2.3 General Photoresponse Properties

Responses are presented in groups called response families (Fig. 5.4 a (Rods) & 5.4 (Cones)). A photoresponse family is several photoresponses gathered with incremental stimulus light intensities. The increasing stimulus light intensity will yield incremental response amplitudes. When the stimulus intensity gets high enough the response amplitude stops growing, the response is said to saturate. If the stimulus intensity is further increased the return of the photoresponse is delayed. The more the stimulus intensity overpasses the saturation threshold the longer the return is delayed. These responses are called supersaturated.

Response amplitudes grow linearly up to 20 % of the saturated photoresponse amplitude. This region is called the ”linear” region and photoresponses of this region are of the same shape. When applying progressively higher light intensities the photoresponses will saturate. Saturation is seen on the ERG as a cessation of amplitude growth (saturation plateau is dotted line in figures 5.4 (a) (rods) and 5.4 (b) (cones)).

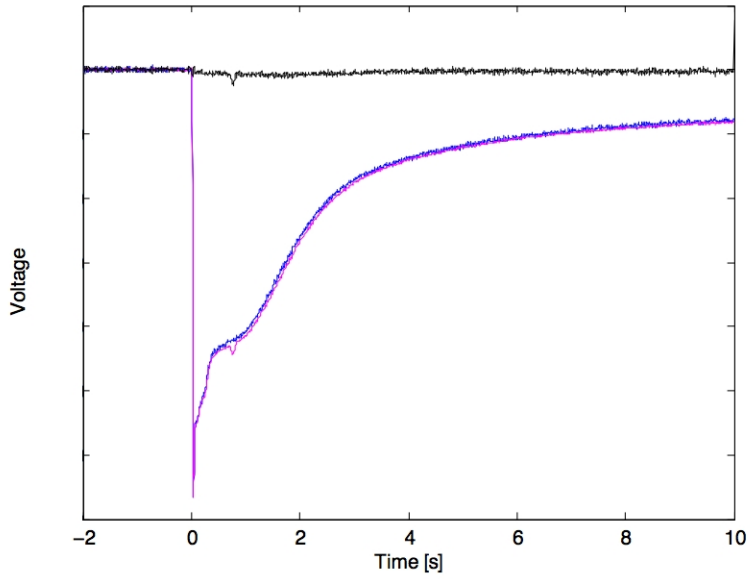

Figure 5.5: Separation of a cone photoresponse from the summed rod-cone response. The saturated rod response (blue curve) is subtracted from the rod-cone photoresponse (purple curve) yielding a resultant cone photoresponse (black curve).

To be able to compare response families with each other they can be normalized. All photoresponses of one family are normalized in respect to the saturation amplitude. The resultant responses are referred to as fractional responses.

The mouse retina consists of 97% rods and 3% cones [8]. The summed ERG-signal signal that originates in rods will therefore be larger. Generally the rod photoresponse kinetics are slower than that of cones'. The rod response duration is longer than the cone's (Fig. 5.4 (a) (Rods) & (b) (Cones)). The mouse rod response's amplitude is larger than the cone's.

5.3 The Recording Protocols

At the beginning of every experiment the incident light-intensity (I_0) was checked.

After dissection of the retina was placed in the specimen holder and superfusion of the Ringer's solution was immediately started. The retina was slowly heated up to 37° C. During this time the retina was continuously monitored by recording flash responses to determine whether the response amplitude and kinetics were stable.

At the beginning of each measurement a family of rod photoresponses are gathered for the purpose of ensuring the normal functioning of the retina. Data such as the rate of inactivation, sensitivity and the time until maximum amplitude in both

rods and cones has already been thoroughly studied and acts as a good indicator on the functioning of the retina.

5.3.1 The Stimulus Protocols

The following stimulus protocols were used to examine different aspects of light adaptation.

Stepped background

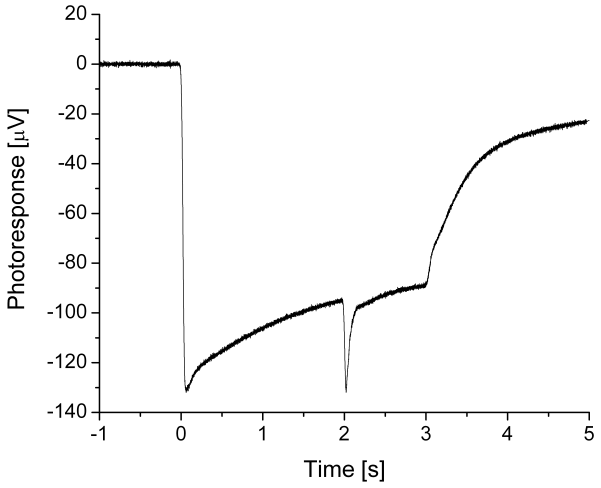

Figure 5.6: A 3000 s rod-saturating step of background light and the test-flash applied 2000 ms into the rod-saturating preflash.

To examine how the cone responses change in response to different background illumination a step flash protocol was used. A step of background light of 3000 ms was applied to keep the rods in saturation. A 2 ms test flash was then recorded during rod saturation (Fig. 5.6).

Constant Background Illumination

A continuous background illumination was turned on about 5 minutes before the response family is taken. The background intensity has to be large enough to completely saturate the rods of the retina. Because of rod saturation the test-flashes elicited only cone photoresponses.

5.4 Analysis

The measurement data were analyzed with the AnaBin (made at Helsinki University of Technology Biophysics Laboratory) and Microcal Origin computer softwares.

In AnaBin the voltage-level before the photoresponse was taken and put to zero (baseline). To improve the signal-to-noise ratio the photoresponses gathered with the same stimulus intensity were averaged. A greater amount of samples were collected at small photoresponse amplitudes compared to large-stimulus responses. The photoresponse data was saved as ASCII-files to be used for later analysis. The subsequent analysis was done with the Microcal Origin software.

5.4.1 Fractional Responses

To make photoresponses from different response families comparable with each other the responses can be normalized in respect to the saturation amplitude. The responses normalized in this way are called fractional responses $F(t)$:

$$F(t) = \frac{r(t)}{r_{max}}, \tag{5.8}$$

where $r(t)$ is the photoresponse, r_{max} is the saturation amplitude.

5.4.2 Amplitude vs. intensity plots

The amplitude vs. intensity data visualize the photoreceptor's dynamical operating area, which shifs as a function of intensity of the background illumination. The fractional amplitude $\frac{r(t_p)}{r_{max}}$ describes the photoresponses maximum amplitude $r(t_p)$ normalized to the photoreceptors saturation amplitude r_{max}. This data was fitted to the following function:

$$\log_{10}\left[\frac{r(t_p)}{r_{max}}\right] = \log_{10}\left[a \cdot \frac{I_F}{I_F + I_{\frac{1}{2}}} + (1-a)(1-e^{-S_F \cdot I_F})\right], \tag{5.9}$$

where I_F is the flash intensity and $I_{\frac{1}{2}}$ is the intensity needed for half saturation of the photoreceptor. $I_{\frac{1}{2}}$ is inversely proportional to the fractional sensitivity S_F.

$$S_F = \frac{1}{I_{\frac{1}{2}}} \tag{5.10}$$

Two functions that approximately follow the amplitude-intensity data-points have been constructed: the Michaelis function and a function that describes the amplitude growth as exponential. Both of these are present in equation 5.9. The first part of the function equals the Michaelis function (Eq. 5.11). The second part the

exponential. The parameter a ($a \in [0, 1]$) describes the weighting each of these function has when the data is best fitted.

Experience has shown that cone's amplitude-intensity data fit better to the Michaelis function [9].

$$\frac{r(t_p)}{r_{max}} = \frac{I_F}{I_F + \frac{1}{S_F}} \tag{5.11}$$

The stimulus intensity $I_{\frac{1}{2}}$ needed to reach an amplitude half of the saturation amplitude is inversely proportional to the S_F (Eq 5.10). The fractional sensitivity S_F describes the fraction of photocurrent turned off by a single photon (if the S_F is expressed in photoisomerizations). The stimulus intensities are given in either photons h$\nu_\lambda \mu m^{-2}$ or number of isomerized pigments per cell (R*).

The mammalian rod data at body temperature, on the other hand, better fit to the exponential part of equation 5.9. In saturated mouse rods there is a nose component (Chapter 4.1.5) is present. The following plateau, however, believed to reflect from the saturation of the rod. When fitting the rod data to equation 5.9 the parameter a becomes close to zero and the first part of the function (the Michealis function) is eliminated from the expression. The rod data thus fits to equation 5.12.

$$\frac{r(t_p)}{r_{max}} = 1 - e^{-S_F \cdot I_F} \tag{5.12}$$

5.4.3 Dominant Time Constant of Recovery

The dominant time constant of recovery (τ_{rec}) describes saturated photorespose deactivation kinetics. The idea behind the calculation of this parameter is: The greater the intensity is the longer time will pass before the deactivation mechanisms overpower the activation mechanisms. In other words, the time the photoreceptor is in saturation grows as the intensity increases. τ_{rec} describes the mechanisms of the slowest phototransduction deactivation mechanism, the so-called rate-limiting kinetics. Calculation of τ_{rec}: The delay time (T_c) that precedes the recovery to a certain criterion amplitude is related to the natural logarithm of the stimulus intensity. For low intensities the saturation time grows linearly with $ln(I_f)$. As $ln(I_f)$ grow T_c's growth decreases to finally stop growing all together. The proportionality constant τ_{rec} between T_c and $ln(I_f)$ describes the exponential decay of photoresponse deactivation. [47]

Chapter 6

Results

Mass response electroretinogram (ERG) was recorded across isolated mice retinae at a temperature of 37 °C. The photorespone b-wave and slow PIII component were pharmacologically blocked resulting in a pure fast PIII photoresponse.

Until recently no studies of mouse cones had been conducted. Mouse cone light adaptation studies have not been pursued at all. The study of light adaptation requires the retina to stay stable longer than e.g. in the study of dark-adapted cone kinetics. The recording of 37 °C brings about a high metabolic activity, leading to a tendency of the retinal pH to fall during the measurement. The pH of the Ringer's solution was therefore raised from the typical value of 7.5 to 7.8.

6.1 Dark adapted Rods and Cones

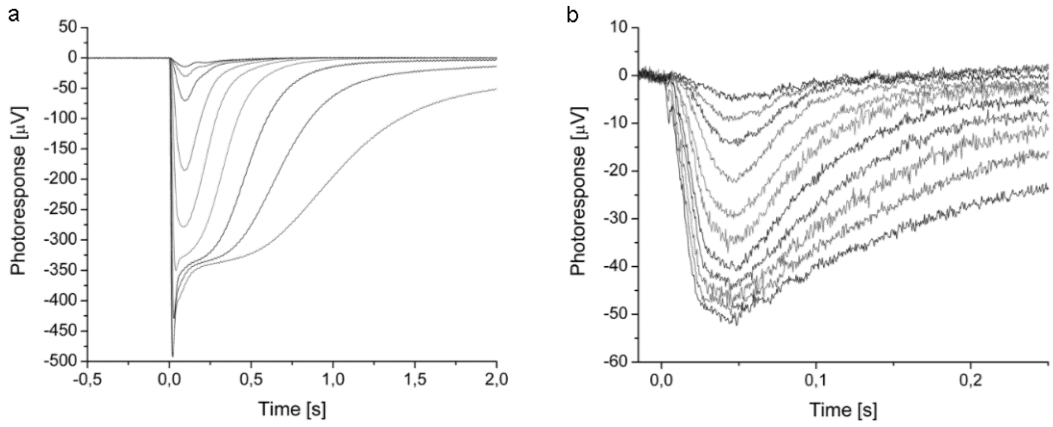

Figure 6.1: **(a)** Averaged dark adapted rod response family. The stimulus intensities (I_F) were 10, 16, 33, 103, 330, 1000, 3300, 10000 and 33000 $h\nu_{\lambda^{-}max}\mu\text{m}^{-2}$ respectively. **(b)** Dark adapted rod response family. The stimulus intensities were 2 000, 4 000, 8 000, 16 000, 32 000, 64 000, 130 000, 250 000, 500 000, 1 000 000, and 2 000 000 $h\nu_{\lambda^{-}max}\mu\text{m}^{-2}$.

Dark-adapted rod and cone photoresponse families (from the same retina) are presented in figure 6.1. (The rod photoresponses collected in the mesopic intensity region also contain a cone component.)

The rod sensitivity is much higher compared with cones. This can also be seen in the intensity versus amplitude plots seen in fig. 6.2. The cone intensity vs. amplitude data best fit to the Michaelis model (Eq. 5.11) for every single retina measured whilst the corresponding rod data better follows an exponential increase in amplitude with incremental illumination (Eq. 5.9). The cone data for one retina presented in figure 6.2 (b) fit best to the Michaelis function and had a half-saturating intensity $I_{\frac{1}{2}} = 12800\ h\nu_{\lambda_{max}}\mu\text{m}^{-2}$ (corresponding to a sensitivity $S = 80 \cdot 10^{-6}\quad (h\nu_{\lambda_{max}}\mu\text{m}^{-2})^{-1}$). The rod data of the same retina (Fig. 6.2 (a)) fit well with the exponential model and had a much lower half-saturating intensity of $I_{\frac{1}{2}} = 170\ h\nu_{\lambda_{max}}\mu\text{m}^{-2}$ ($S = 5800 \cdot 10^{-6}\quad (h\nu_{\lambda_{max}}\mu\text{m}^{-2})^{-1}$). For all the measured retinas the average $I_{\frac{1}{2}} = 15000 \pm 1400\ h\nu_{\lambda_{max}}\mu\text{m}^{-2}$ for cones (n=4) and $I_{\frac{1}{2}} = 140 \pm 26\ h\nu_{\lambda_{max}}\mu\text{m}^{-2}$ for rods (n=2).

The rod photoresponse duration is generally longer compared to cones,indicating that both activation and deactivation are slower in rods. Generally rod large-stimulus responses display a distinct “nose” component while it is much more subtle in cones if apparent at all. In our measurements only one retina showed a nose component in cone responses. The time to reach maximum amplitude was on average $t_p = 90.2 \pm 1.8$ ms (SEM) for rods (n=4). The kinetics of cone responses are much faster and their average $t_p = 45 \pm 1.2$ ms (n=4).

The dominant time constant of recovery (τ_{rec}) reflects the speed of phototrans-

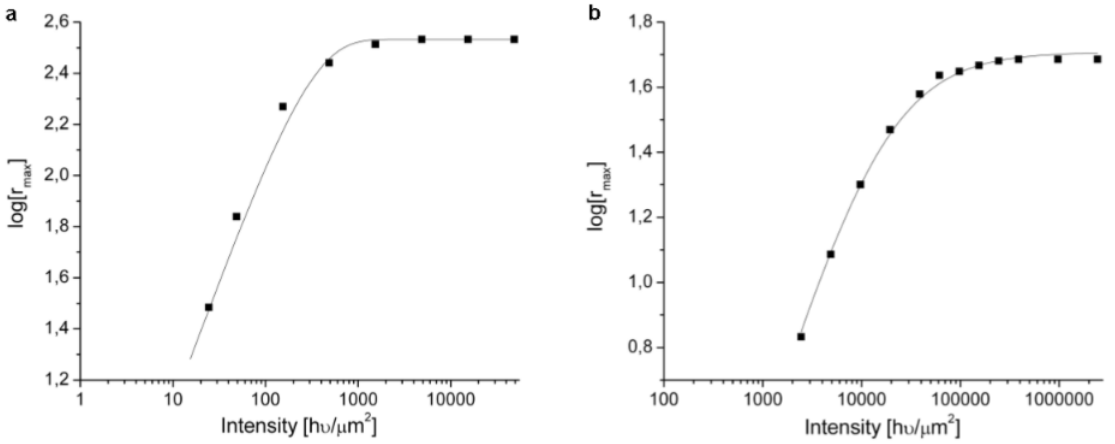

Figure 6.2: **(a)** Amplitude vs. stimulus intensity curve of the rod response in figure 6.1 (a). The continuous curve is the exponential function of eq. 5.12. The fitting yielded $U_{max} = 341\ \mu V$ and $S = 5\ 790 \cdot 10^{-6}\quad (h\nu_{\lambda_{max}}\mu\text{m}^{-2})^{-1}$. **(b)** Amplitude vs. stimulus intensity curve of the cone photoresponses in figure 6.1 b. The continuous curve is the Michaelis function (Eq. 5.11). The fitting yielded $U_{max} = 51\ \mu V$ and $S = 78 \cdot 10^{-6}\quad (h\nu_{\lambda_{max}}\mu\text{m}^{-2})^{-1}$.

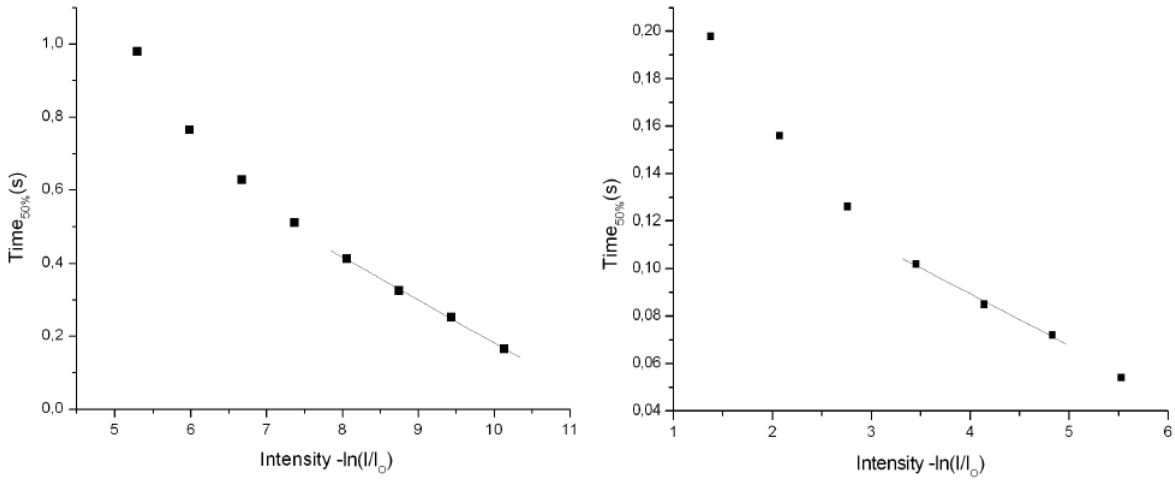

Figure 6.3: Pepperberg plots that display the deactivation kinetics of rods and cones. The time of recovery was measured 50 % of recovery. **(a)** The Pepperberg-plot of rods. The dominant time constant τ_{rec} = 118 ms. I_F = 16-33000 $h\nu_{\lambda^{-}max}\mu\text{m}^{-2}$ **(b)** The Pepperberg-plot of cones. τ_{rec} = 22 ms. I_F = 32 000-2 000 000 $h\nu_{\lambda^{-}max}\mu\text{m}^{-2}$.

duction deactivation. A Pepperberg plot giving τ_{rec} for both rods and cones is displayed in figure 6.3 (with a time of recovery of 50%). For rods τ_{rec}= 110± 4 ms (n=4) and for cones τ_{rec}=40± 7 ms (n=4)

6.2 Light-adapted Cones

To study the mouse cone light adaptation cone photoresponse families were collected under several background illuminations. Two different measurement protocols were used (for more specific information section 5.3.1). In the first method a shorter conditioning (rod-saturating) step of about 3 s was applied, used as the background (step flash protocol). The test flash was taken 2 s into the conditioning flash. In the second protocol, a steady background illumination was turned on about 5 minutes prior to photoresponse family collection. This method allows for the effect of slower light adaptation mechanisms to take effect, such as protein translocation. The reliability of this data, though, is somewhat questionable, due to the divergence of the determined parameters (See discussion). It is still displayed for comparison.

When studying light adaptation the parameters of interest are the changes in the response kinetics and sensitivity. The following parameters have been studied in order to quantify the effects of light adaptation: The dominant time constant τ_{rec} reflects the speed of deactivation. Time to peak (amplitude) t_p is affected by both the activation and deactivation kinetics. The other main manifestation of light adaptation is sensitivity loss. The light induced decline in sensitivity is also put

into numbers.

6.2.1 Stepped Background

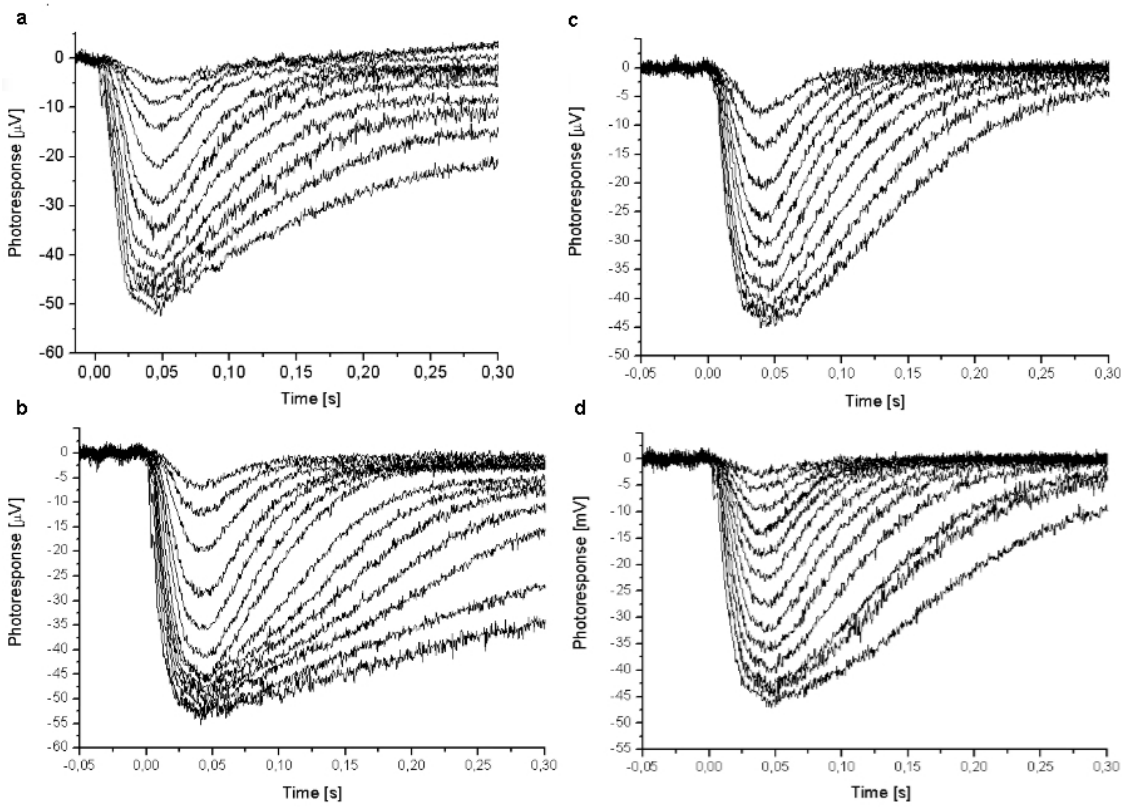

Figure 6.4: Cone ERG photoresponse families recorded in backgrounds **(a)** I_B = 0 **(b)** 110 000 **(c)** 340 000 **(d)** 1 100 000 $h\nu_{\lambda_{max}}/s \cdot \mu\text{m}^2$

Figure 6.4 presents cone photoresponse families in darkness and three stepped adaptive backgrounds.

The cone amplitude-intensity curves for cones in several backgrounds are presented in figure 6.5 for one retina. Totally, two retinas were used to examine cone light adaptation with the step flash protocol. In both cases the amplitude-intensity data fit well with the Michaelis function (Eq. 5.11) also in the light adapted state.

The amplitude vs. intensity plots are presented in figure 6.5, panel (a) presents the logarithm of the amplitudes and panel (b) displays the logarithm of the fractional amplitudes versus stimulus intensity. The amplitude-intensity curve depicts the sensitivity fall as a function of the stimulus intensity. Light adapted amplitude-intensity curves are shifted to the right, which translates into a lower intensity (or an elevation of the half-saturating intensity,$I_{\frac{1}{2}}$). The cone sensitivity appears to be unaffected by weak background illumination or even increase marginally

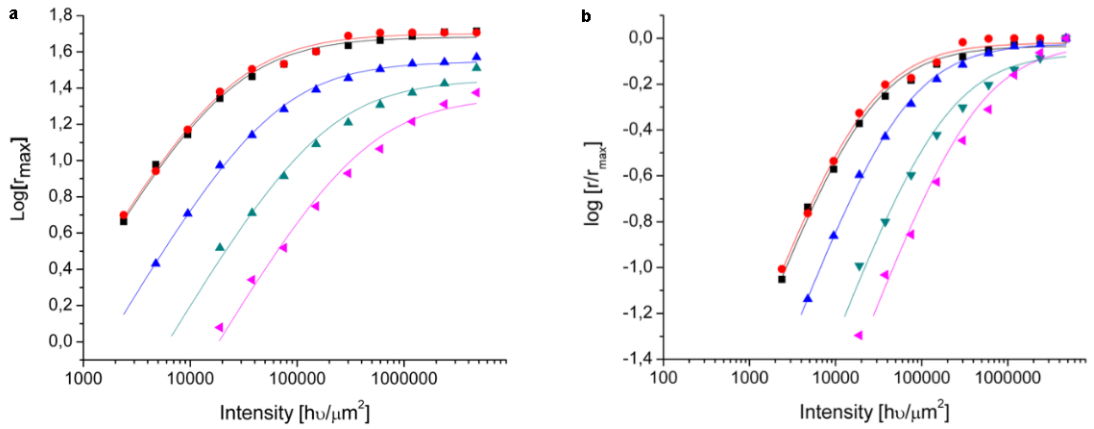

Figure 6.5: **(a)** Amplitude-intensity curves (Eq. 5.11) for cones in several background illuminations. I_B = Dark-adapted (black), 102 000 (red), 324 000 (red), 1 025 000 (green), and 3 241 000 (magenta) $h\nu_{\lambda_{max}}/s \cdot \mu\text{m}^2$. U_{max}= 48, 50, 35, 28, and 22 μV respectively. **(b)** Amplitude-intensity curve from same retina as in figure a, but responses are fractional.

compared to the sensitivity in darkness. When the background intensity further increases, the sensitivity will start dropping.

Weber's law (Eq. 3.1) was fitted to the sensitivity changes due to light exposure. The fit is depicted in figure 6.6 (unbroken curve). When examining normalized responses (linear range) at fixed stimulus intensity collected in increasing background illumination the effects of sensitivity loss can be observed as a drop in amplitude. Photoresponses collected with an unchanged stimulus intensity in the linear range decreased in amplitude as the background intensity increased (Fig. 6.7), with the exception of the dimmest background. There the amplitude actually grew somewhat.

Table 6.1: The change in cone sensitivity (S) due to background illumination (n=2).

Background $[h\nu_{\lambda_{max}}/s \cdot \mu\text{m}^2]$	$S\pm$ SEM $[10^{-6} \cdot (h\nu_{\lambda_{max}}\mu\text{m}^{-2})^{-1}]$
Dark	66 ±7
110 000	67 ± 10
340 000	24±2
1 100 000	8 ±1

When cones were subjected to increasing background illumination t_p of small-stimulus responses decreased as represented in figure 6.8 (a). The figure shows that the lowest background does not seem to be able to light adapt the cones. The dominant time constant of recovery also changed in response to background illumination (Fig. 6.8 (b)). Figure 6.9 a & b displays the Pepperberg plots from which τ_{rec} was determined. No unambiguous rise or fall of τ_{rec} in relation to increasing

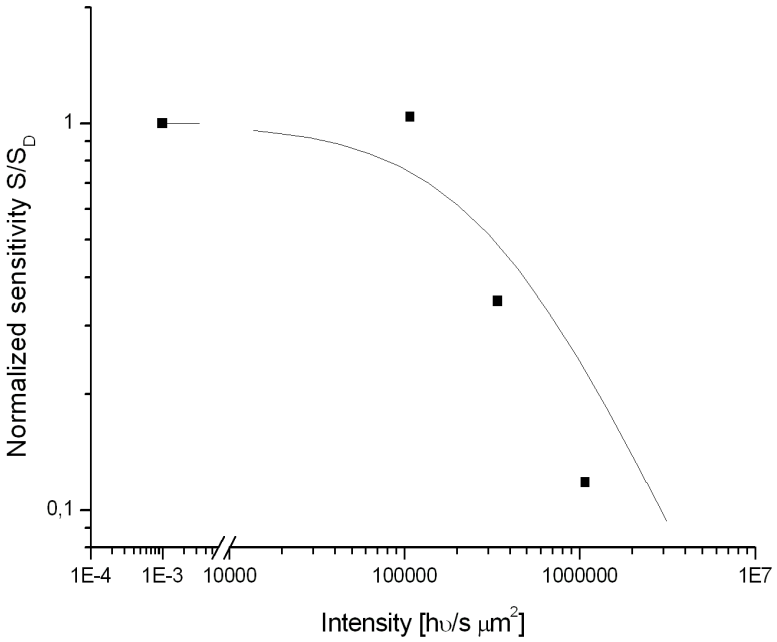

Figure 6.6: The closed squares depict sensitivity S in a certain background illumination. The unbroken curve depicts the Weber's law-fit.

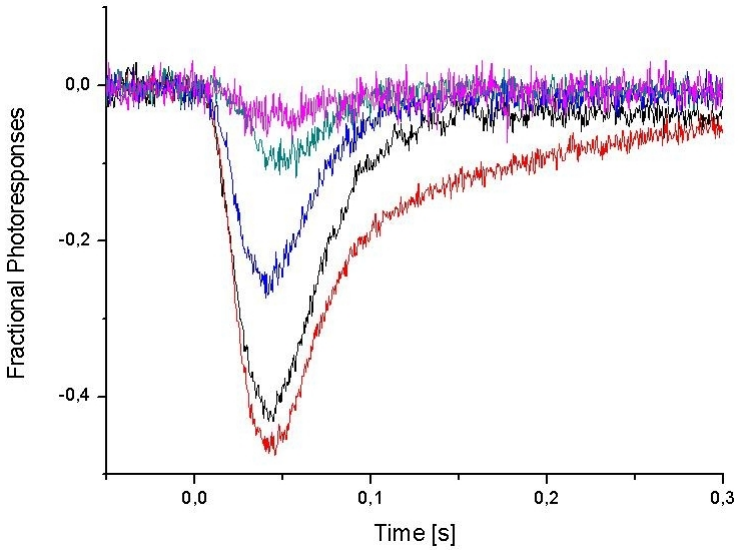

Figure 6.7: Average responses normalized with the dark-adapted response amplitude (U_{Dark}) gathered at fixed stimulus intensity (I_F = 16 000 $h\nu_{\lambda_{max}}\mu\text{m}^{-2}$) in progressively brighter backgrounds. Background intensities I_B darkness (black), 82 000 (red), 260 000 (green), 820 000 (blue), 2 600 000 $h\nu_{\lambda_{max}}/s \cdot \mu\text{m}^2$ (cyan).

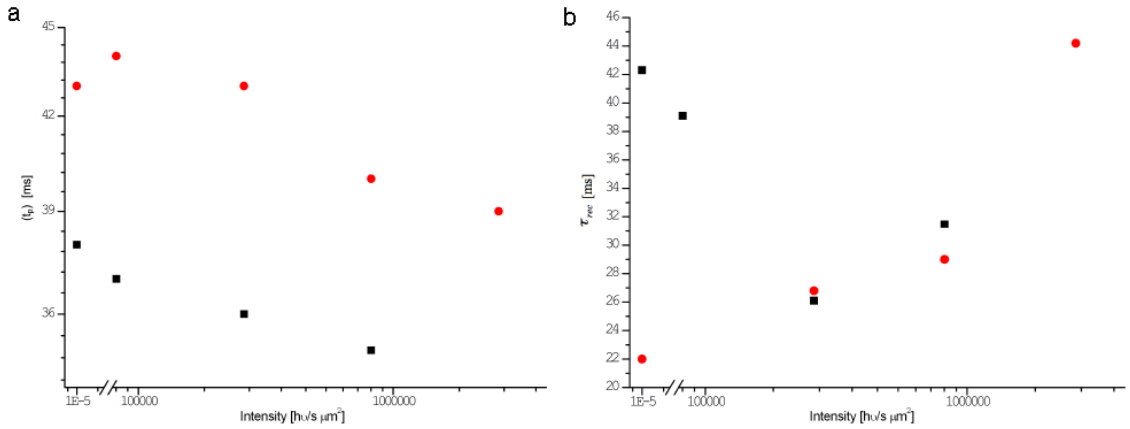

Figure 6.8: The effect of background light on cone **(a)** t_p and **(b)** τ_{rec} from two retinas (backgrounds I_B = 0, 82 000, 260 000, 820 000 and 2 600 000). Black squares = retina 1, red circles retina 2.

background illumination could be determined from the measurements (n=2). τ_{rec} calculated from one retina grew monotonously as the background intensity was increased, whilst the other measurement gave a τ_{rec} that first decreased to start growing at the larger backgrounds (see Discussion).

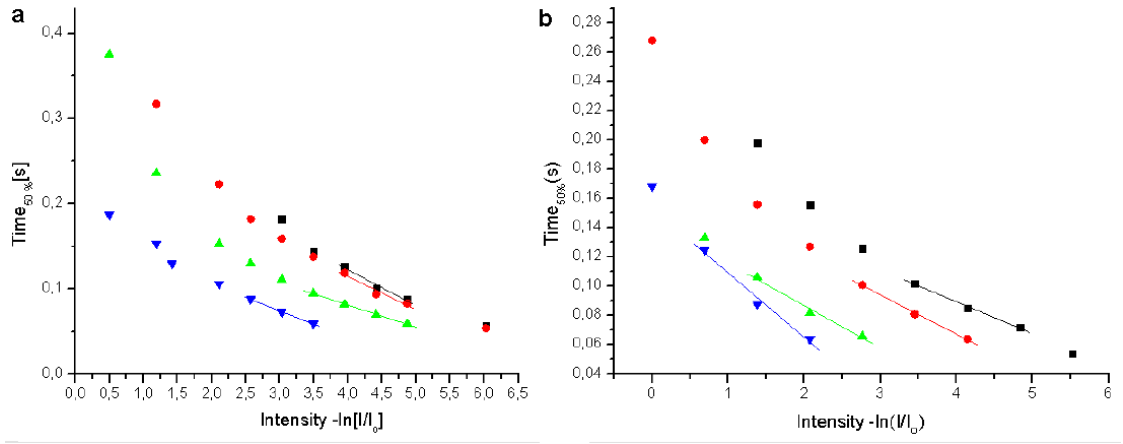

Figure 6.9: Pepperberg plots in darkness and in three adaptive continuous backgrounds. **(a)** Retina 1. Stimulus intensities I_S = 8 100 - 4 100 000 $h\nu_{\lambda_{max}} \cdot \mu\text{m}^{-2}$. I_B = 0 (black), 82 000 (red), 260 000 (green), 820 000 (green) $h\nu_{\lambda_{max}}/s \cdot \mu\text{m}^2$. **(b)** Retina 2. Stimulus intensities I_S = 16 000-4 000 000 $h\nu_{\lambda_{max}} \cdot \mu\text{m}^{-2}$. I_B = 0 (black), 82 000 (red), 260 000 (green), 820 000 (green) $h\nu_{\lambda_{max}}/s \cdot \mu\text{m}^2$.

6.2.2 Continuous Backgrounds

Figure 6.10 presents cone photoresponse families in darkness and three stepped adaptive backgrounds. While the photoresponses recorded during stepped background should reflect the light adaptation mechanisms (that take effect after few seconds), continuous background illumination should also reflect the characteristics of slower adaptational mechanisms (that take effect after a few seconds to up to about 5 minutes).

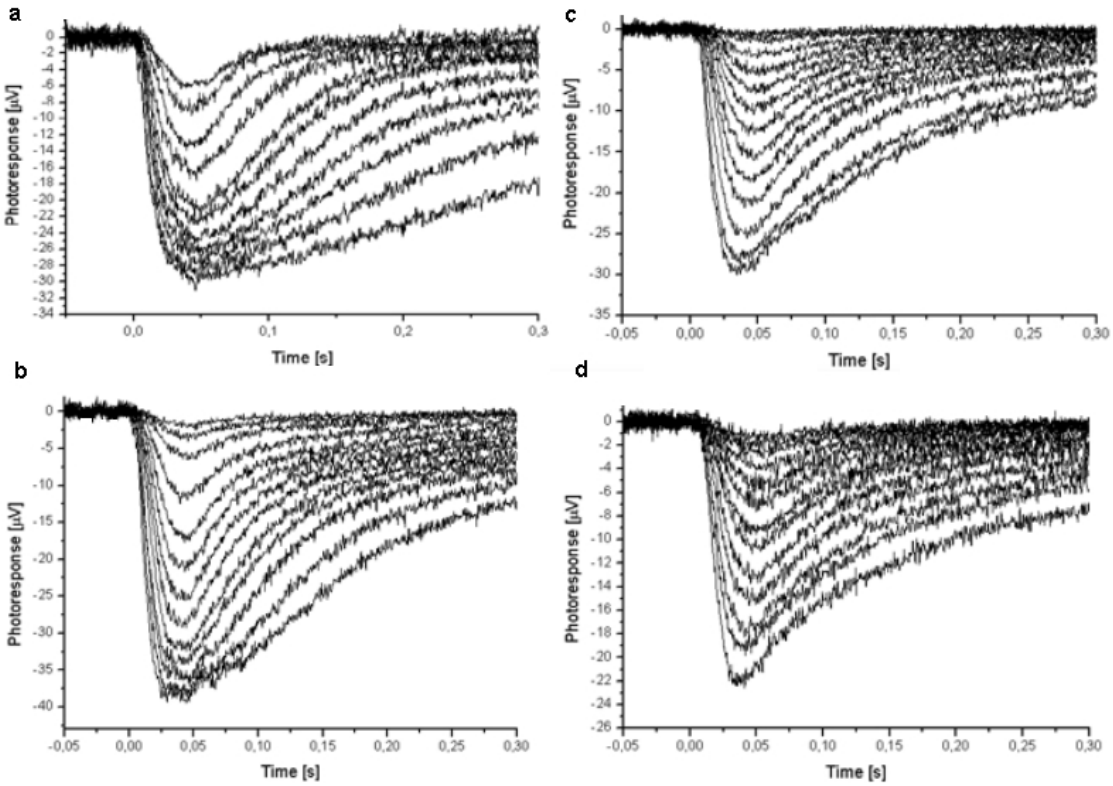

Figure 6.10: Cone ERG photoresponse families recorded in darkness and in three adaptive continuous backgrounds **(a)** $I_B = 0$ **(b)** 82 000 **(c)** 260 000 **(d)** 820 000 $h\nu_{\lambda_{max}}/s \cdot \mu\text{m}^2$

Figure 6.11 depicts photoresponse behavior in incremental background illumination (while the stimulus intensity is fixed). The photoresponse kinetics did differ somewhat from the kinetics of the flash responses imposed on stepped backgrounds (previous section). The cone sensitivities of the continuous background illumination measured are listed in table 6.2. When compared to the experiments performed with stepped backgrounds the sensitivity dropped significantly more, e.g. at an illumination of 107 800 $h\nu_{\lambda_{max}}/s \cdot \mu\text{m}^2$ the S=24$\cdot 10^{-6} \cdot (h\nu_{\lambda_{max}}\mu\text{m}^{-2})^{-1}$ (n=1) in the continuous background in comparison to S=67$\pm$10$\cdot 10^{-6} \cdot (h\nu_{\lambda_{max}}\mu\text{m}^{-2})^{-1}$ (n=1). The bigger drop is certainly expected, since the retina is subjected to a significantly larger amount of light when the light source is continuously on (Pigment bleaching, see Discussion).

Table 6.2: The change in cone sensitivity (S) in response to continuous background illumination. (n=2)

Background $[h\nu_{\lambda_{max}}/s \cdot \mu\text{m}^2]$	$S \quad [10^{-6} \cdot (h\nu_{\lambda_{max}}\mu\text{m}^{-2})^{-1}]$
Dark	81
110 000	24
340 000	6.3
1 100 000	2.0

The time to peak amplitude (t_p) grew in response to continuous background light for every single retina (n=3) measured (Tab. 6.3). τ_{rec}, on the other hand, did not display any clear trend of growth or decline (Tab. 6.4).

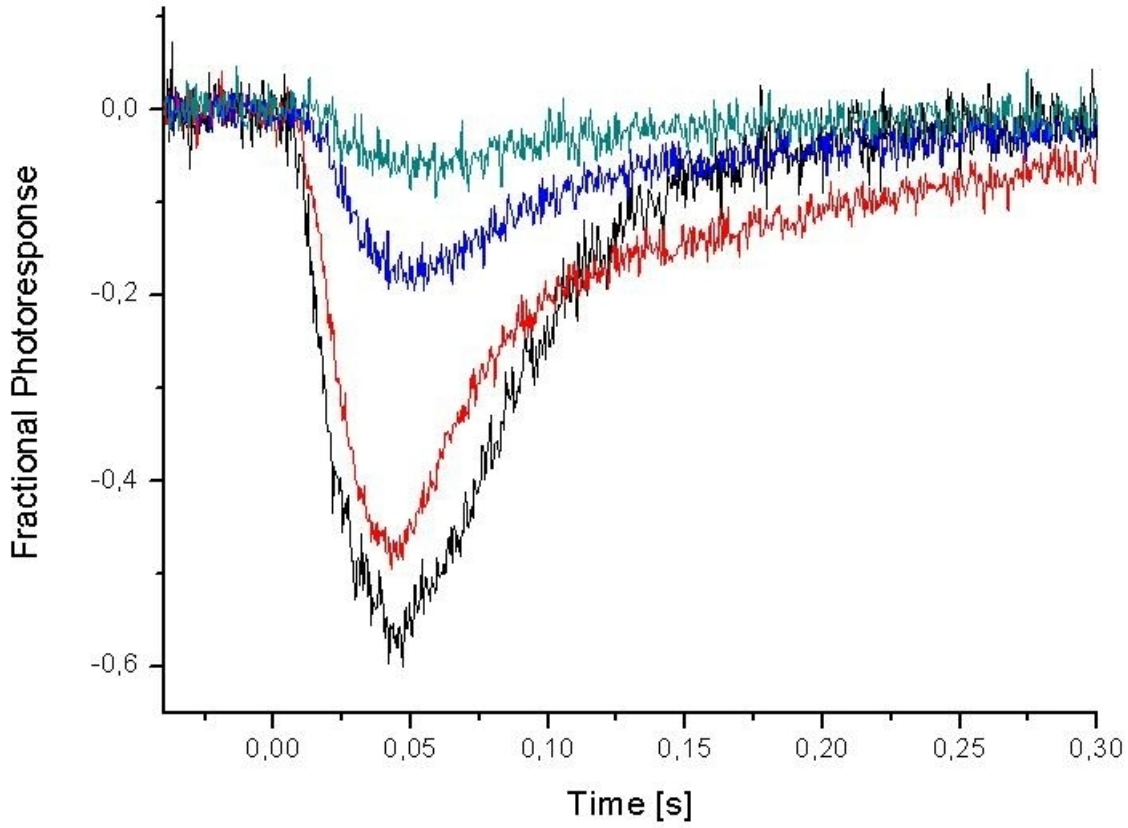

Figure 6.11: Fractional photoresponses from progressively brighter backgrounds. I_F = 32 000 $h\nu_{\lambda_{max}}\mu\text{m}^{-2}$. I_B = 0 (Black), 82 000 (Red), 260 000 (Green), and 820 000 (blue) $[h\nu_{\lambda_{max}}/s \cdot \mu\text{m}^2]$. (Retina 3)

Table 6.3: t_p of three retinas in response to continuous background illumination.

t_p [ms] Background $[h\nu_{\lambda_{max}}/s \cdot \mu\text{m}^2]$	Retina 1	Retina 2	Retina 3
Dark	46	52	45
82 000	–	–	43
260 000	–	–	46
340 000	51	53	–
820 000	–	–	51
1 100 000	59	81	–

Table 6.4: τ_{rec} of three retinas in response to continuous background illumination.

τ_{rec} [ms] Background $[h\nu_{\lambda_{max}}/s \cdot \mu\text{m}^2]$	Retina 1	Retina 2	Retina 3
Dark	40.5	43	57
82 000	–	–	31
260 000	–	–	30
340 000	35	43	–
820 000	–	–	46
1 100 000	27.3	43	–

6.3 α-transducin Knockout Mouse

6.3.1 Dark Adapted Photoresponses

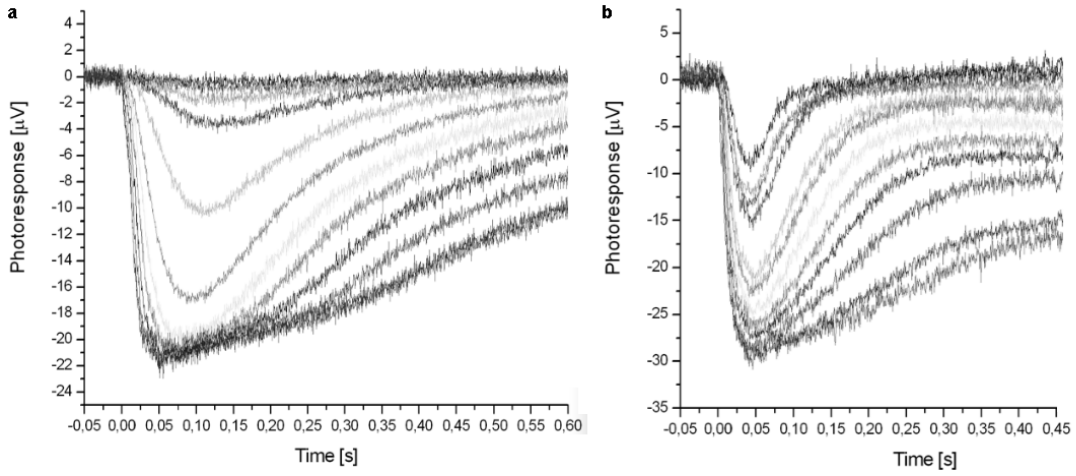

Figure 6.12: **(a)** Averaged dark-adapted photoresponse family from a Tr$\alpha -/-$ mouse. I_F = 880, 1 800, 3 500, 7 000, 22 100, 44 000, 88 000, 180 000, 350 000, 700 000, 1 400 000, 2 800 000 $[h\nu_{\lambda_{max}}/s \cdot \mu\text{m}^2]$ **(b)** WT dark-adapted cone response family. I_F = 2 100, 4 100, 8 200, 16 000, 33 000, 52 000, 82 000, 130 000, 210 000, 330 000, 520 000, 1 100 000, 2 100 000 $[h\nu_{\lambda_{max}}/s \cdot \mu\text{m}^2]$. Both photoresponse families are displayed in the same time scale.

A mouse, which has its rod α-transducin gene knocked out, was engineered to have functionless rods. Such a mouse, which potentially would only yield a photoresponse originating from cones, would facilitate the examination of cones.

Figure 6.12 compares photoresponses of an α-transducin knockout mouse (Tr$\alpha -/-$) with a wild type (WT) one. The Tr$\alpha -/-$ photoresponse duration is significantly longer compared to the WT mouse photoresponse. The activation as well as the deactivation phase were clearly retarded, t_p for WT cones was 44 $\pm$ 2 ms and for Tr$\alpha -/-$ photoreceptors t_p = 128 ms (dark adapted). The later value of t_p is typical for rods (see section 6.1). However, the time constant of recovery τ_{rec} was typical for WT cones. τ_{rec} for the Tr$\alpha -/-$ mouse was 51 ms (n=1) compared to 40$\pm$ 7 ms (n=4) for WT cones and 110 $\pm$ 4 ms (n=4) for rods. The nose component, which is very prominent in supersaturated rod photoresponses, is not apparent in the Tr$\alpha -/-$ photoresponse.

As implied earlier, the amplitude-intensity data of WT mouse cones usually has a good fit to the Michaelis function. All the data available to date, both for dark [9] and light adapted mouse cones (this thesis, see section 6.2.1), indicate that the Michaelis function does indeed depict photoresponse amplitude growth in response to flashes of increasing intensity. In contrast, the amplitude-intensity fit in the case of Tr$\alpha -/-$ photoreceptors coincided better with the exponential curve

(Eq. 5.12), as is typical for mice rods (37 °C).

Furthermore, the photoreceptor sensitivity was lower compared to WT cones. Tr$\alpha -/-$ photoreceptors had a $S = 29 \cdot 10^{-6} h\nu_{\lambda_{max}} \mu\text{m}^{-2}$ (n=1) and WT cone $S = 66 \pm 7 \cdot 10^{-6} h\nu_{\lambda_{max}} \mu\text{m}^{-2}$ (n=2). The Tr$\alpha -/-$ photoreceptors sensitivity did neither correspond with wild type rod $S = 0.007 \pm 0.001$ $(h\nu_{\lambda_{max}} \mu\text{m}^{-2})^{-1}$ (n=2).

6.3.2 Light Adaptation of Tr$\alpha -/-$ Photoreceptors

Figure 6.13 presents cone photoresponse families in darkness and three stepped adaptive backgrounds.

The sensitivity does fall (Tab. 6.5, Fig. 6.14) in response to background illumination. This might indicate that light adaptation does somehow occur in the Tr$\alpha -/-$ photoreceptors. However, the sensitivity data does not fit to the Weber function (Fig. 6.15) nor does the behavior in the fall in sensitivity resemble the WT cone sensitivity fall (Fig. 6.6).

The sensitivity-drop of the Tr$\alpha -/-$ photoreceptors is evident when examining fractional photoresponses (Fig. 6.16). In accordance with light adaptation and desensitization there is an amplitude decrement connected to a rise in background illumination.

Background light exposure did not cause t_p of Tr$\alpha -/-$ photoresponses to decline. At the lowest backgrounds used t_p instead started growing (Tab. 6.5). But, at the brightest background t_p again decreased back to the dark-adapted value (see discussion).

The recovery also follows the same pattern: a more and more retarded recovery of the response as the background brightness increases. As seen in table 6.5 τ_{rec} (its Pepperberg plot in Fig. 6.17) grows with increasing background illumination. τ_{rec} also follows the same trend as t_p. It decreases in the brightest background.

Table 6.5: Flash response parameters of Tr$\alpha -/-$ mice. (n=1)

Background $[h\nu_{\lambda_{max}}/s \cdot \mu\text{m}^2]$	τ_{rec} [ms]	t_p [ms]	S $[10^{-6} \cdot h\nu_{\lambda^-max} \mu\text{m}^{-2}]$
Darkness	51	128	29
51	58	136	17.3
160	72	136	14.8
510	87	143	10.5
1 600	80	127	9.5

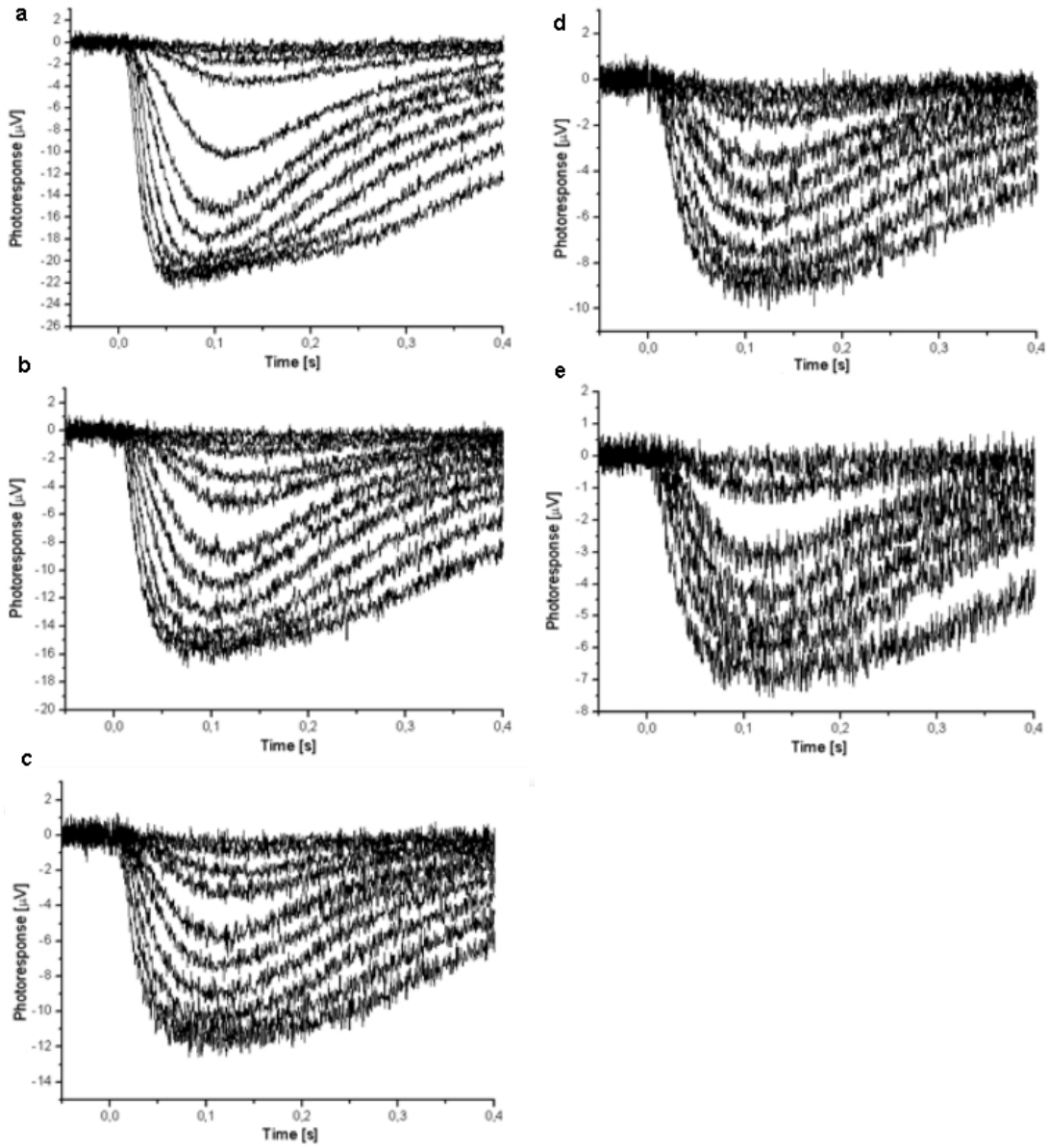

Figure 6.13: Trα photoreceptor ERG photoresponse families recorded in darkness and in three adaptive stepped backgrounds **(a)** $I_B = 0$ **(b)** 51 **(c)** 160 **(d)** 510 **(e)** 1600 $h\nu_{\lambda_{max}}/s \cdot \mu\text{m}^2$

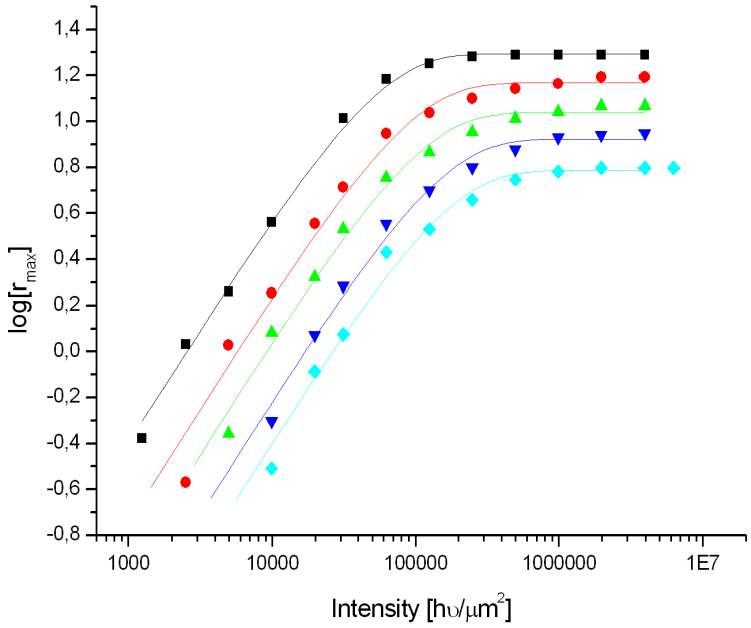

Figure 6.14: Amplitude-intensity curves collected in several background lighting levels. I_B = 50, 160, 500, 1 600 $[h\nu_{\lambda_{max}}/s \cdot \mu\text{m}^2]$. The results were fit to Eq. 5.12 (exponential model). U_{max} = 20, 15, 11,8 and 6 μV respectively

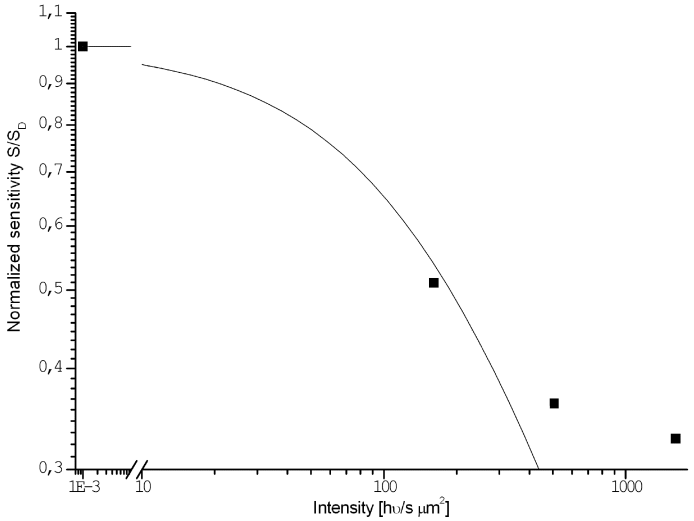

Figure 6.15: The sensitivity vs. background illumination data. The unbroken line represents the Weber function fit to the data points.

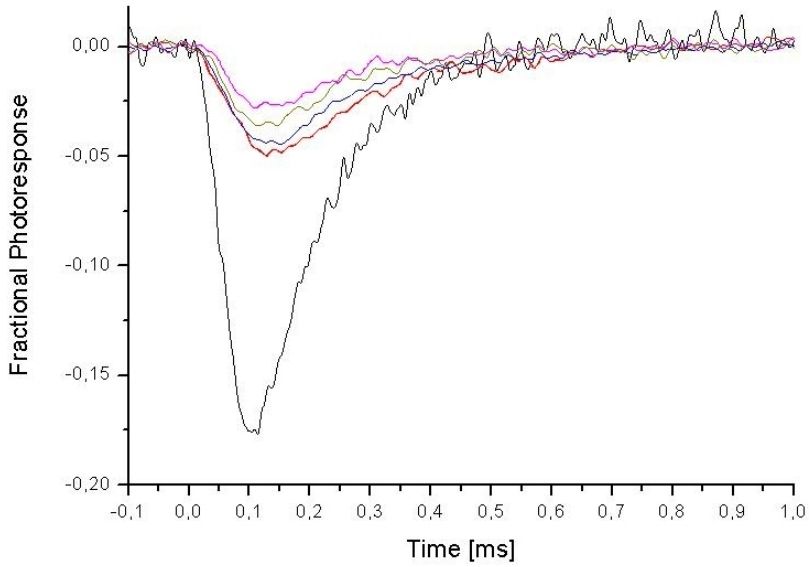

Figure 6.16: Fractional photoresponses gathered in incremental background illumination with a fixed stimulus flash intensity. Background intensities are I_B = 50, 160, 500, 1 600 $[h\nu_{\lambda_{max}}/s \cdot \mu\text{m}^2]$. Flash intensity is I_F = 7 000 $h\nu_{\lambda_{max}}\mu\text{m}^{-2}$.

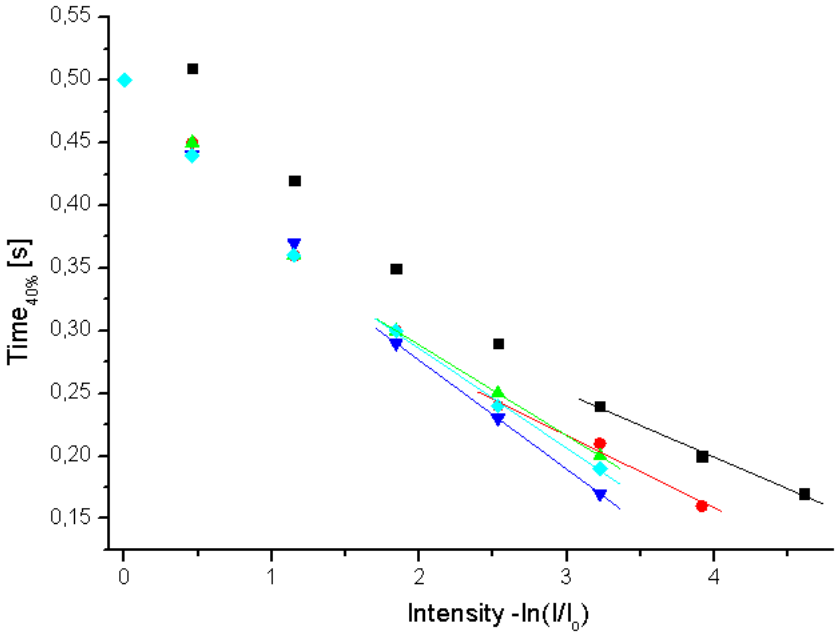

Figure 6.17: Pepperberg plots in darkness and in three adaptive continuous backgrounds. Stimulus intensities I_S = 44 000 - 2 800 000 $h\nu_{\lambda_{max}} \cdot \mu\text{m}^{-2}$. I_B = 0 (black), 51 (red), 160 (green), 510 (cyan), 1 600 (blue) $h\nu_{\lambda_{max}}/s \cdot \mu\text{m}^2$.

Chapter 7

Discussion

In this study, the number of retinas recorded from in each type of experiment was low. In order to determine more reliable values for the parameters of interest, more experiments have to be conducted. However, the results of this study give some preliminary findings about cone light adaptation, facilitating its further examination.

7.1 Rod and Cone a-wave Characteristics

When comparing the mouse photoresponse (isolated fast PIII component) parameters to an earlier work [9] a general observation is that the response kinetics of dark-adapted photoreceptors were somewhat faster. The corresponding parameter values from this study and the study of Heikkinen *et al.* [9] are summarized in table 7.1 for comparison.

Often the stimulus intensity is given as the number of isomerizations produced by a certain amount of light. In this thesis the light intensity values were chosen to be displayed as the incoming amount of photons per μm^{-2} ($h\nu_{\lambda^-max}\mu$m^{-2}). The reason for this choice was that it was difficult to compute the number of photoisomerizations in the light adapted case. This was due to the fact that it was difficult to determine the amount of unbleached pigment available (especially for the high

Table 7.1: A comparison of photoresponse parameters obtained in this study and in the study of Heikkinen et al. [9] *Time of 50-60 % recovery. **Time of 20% recovery

Parameter	**This thesis**		**Heikkinen *et al.***	
	Rod	Cone	Rod	Cone
t_p [ms]	90 $\pm$ 2	45 $\pm$ 1	117 $\pm$ 3	51 $\pm$
τ_{rec} [ms]	110 $\pm$ 4 ms*	40$\pm$ 7 *	160 $\pm$ 7**	33 $\pm$ 4**
$I_{\frac{1}{2}}$ [$h\nu_{\lambda_{max}}\mu$m^{-2}]	140 $\pm$ 26	15 000 $\pm$ 1400	110 $\pm$ 40	5 500 $\pm$ 700

intensities needed for cone light adaptation experiments). The rate of pigment regeneration in both rods and cones of an isolated retina was not known. The removal of the RPE will reduce both photoreceptor types' pigment regeneration. However, some regeneration of cone pigment is performed by the Müller cells. Hence, the amount of unbleached pigment can be concluded to be reduced as the measurement proceeds and retina will desensitize more than under in vivo circumstances. Therefore the estimation of the number of isomerizations is beyond the scope of this thesis.

In mice, the cone photoresponse amplitude is much smaller than the rod response. The signal-to-noise ratio (SNR) is thereby lower and the harm caused by noise is more prominent. In some cases, the isolated cone photoresponse saturation level was hard to determine. Notable, though, is that an error in determining the saturation level a few microvolts in any direction will not affect the outcome of τ_{rec} in any significant way. The determination of τ_{rec} method was originally developed for rod photoresponses [47], which are of different shape (translating into different kinetics) compared to cones. Some cone photoresponse (ERG) families were of such shape that it was difficult to determine τ_{rec} time to 20 % of response return. Depending on the photoresponse family shape a time of 40-60 % response return was used in this study. Consequently some of the photoresponses that had to be used were not saturated, though they were very close to saturation.

7.2 Light Adaptation

The study of cone adaptation can be conducted in a number of ways. Because of the complexity of the molecular mechanisms of this phenomenon it would be of utter importance to choose a method of investigation that correctly reflects changes caused by light adaptation. In this study two alternative types of backgrounds were used, a continuous and stepped background illumination.

A continuous background illumination will cause slower light adaptation mechanisms, such as protein translocation, to get fully activated. The big amount of light applied will cause the amount of bleached pigment to be considerably larger than under in vivo conditions, when the retina is not isolated. Consequently, the cone sensitivity will probably drop more compared to in vivo conditions. If the fall in pigment regeneration rate could be calculated the sensitivity calculations could compensate for this.

In the case of a discontinuous background illumination (the stepped background) the isolated retina will receive less light in total. Thus, pigment bleaching will not be as prominent. However, its role might become more and more apparent as the measurement goes on, i.e. the response families gathered in the brightest background light will be more affected by the pigment bleaching.

The question therefore arises whether the sensitivity data would follow Weber's law, if corrections were made for the pigment bleaching. Nonetheless, Donner *et*

al. 1998 [10] already concluded that their corresponding cone sensitivity (frogs) data did not follow Weber's law. Donner *et al.* suggested that Weber's law would not be applicable on cones. Our data seem to point to the same conclusion. Soo *et al.* (2008) [51], on the other hand did manage to fit data from salamander L-cones to the Weber function [51] (their fig. 3d). Here, though only a few backgrounds were used and a question arises whether the data would conform to the Weber function if a wider range of backgrounds were taken into account.

In both continuous and stepped backgrounds, the activation and deactivation speeds of mice cones are slowed down in response to increasing backgrounds (stepped background fig. 6.7, continuous background fig. 6.11). The kinetics of mouse rods also seem to behave differently in stepped vs. continuous backgrounds ([49], their fig. 1 & 6A).

In other species studied (rat rods [50] their fig. 8a and frog cones [48] in continuous background) the activation and deactivation speeds instead do not appear to change. As the backgrounds increase the fractional responses are said to "peel off" a common "activation" curve, i.e. the activation speed does not change but the full force of deactivation instead starts earlier as background illumination is raised (t_p is shortened). The deactivation speed does neither seem to change considerably. [50, 48]

Hence, the changes in kinetics of mice photoresponses modulated by light adaptation seem to differ from some of the other species studied. This could be a reflection of differences in molecular mechanisms or their level of activity.

7.3 α-transducin Knockout Mouse

The examination of mouse cones with ERG is quite laborious because a flash of light in the mesopic region elicits an electrical response from both rods and cones. If mice retinae could be genetically engineered to consist of solely functional cones the study of them would become appreciably facilitated. The thought behind the α-transducin knockout mouse was just that, to create a mouse that only has functional cones.

7.3.1 Dark-adapted Tr$\alpha -/-$ Photoreceptors

In figure 6.12 a Tr$\alpha -/-$ mouse photoresponse family were compared with a wild-type (WT) cone photoresponse family. The overall response kinetics of the Tr$\alpha -/-$ photoreceptors were shown to be much slower compared with WT cones. Nikonov *el al.* (2006) [8] came to the same conclusion. A more in depth examination reveals that both activation and deactivation times are slower compared to WT cones (Section 6.3.1). The slower photoresponse kinetics would indicate a more "rod-like" behavior. However, the supersaturated Tr$\alpha -/-$ photoresponses

do not resemble mouse (WT) rod photoresponses. The most evident dissimilarity between the rod and Tr$\alpha -/-$ photoresponse is in the absence of a distinct nose component of the Tr$\alpha -/-$ responses. The sensitivity of the Tr$\alpha -/-$ photoreceptors, though, were closer to the sensitivity of WT cones than rods (Tr$\alpha -/-$ photoreceptors 29 $\cdot 10^{-6}$ $(h\nu_{\lambda_{max}}\mu\text{m}^{-2})^{-1}$, WT Cones 66 $\pm$ 7 $\cdot 10^{-6}$ $(h\nu_{\lambda_{max}}\mu\text{m}^{-2})^{-1}$ and WT rods 7100 $\pm$ 1200 $\cdot 10^{-6}$ $(h\nu_{\lambda_{max}}\mu\text{m}^{-2})^{-1}$). However, the Tr$\alpha -/-$ photoreceptors were slightly less light sensitive than WT mice M-cones. Nikonov *et al.*'s experimental data also indicate that the Tr$\alpha -/-$ photoreceptors are more light sensitive [8] when compared to WT cones. The difference between Tr$\alpha -/-$ and WT cone sensitivity, though, is small when compared to the magnitude difference between WT rods and cones. An interesting detail worth noting, is the growth in amplitude to incremental light flashes. In this case the data fit the exponential model better (Eq. 5.12). In cones of body temperature this amplitude growth has been found to fit better to the Michaelis function. This does again indicate that the functioning these photoreceptors of rod α-transducin knockout mice do not reflect normal WT mouse cone phototransduction.

Taking all this information into account the conclusion will be that the Tr$\alpha -/-$ photoreceptors do not behave like WT cones. Rather, some of its mechanisms seems to function like cones, while other mechanisms instead display rod-like behavior.

7.3.2 Light Adaptation of Tr$\alpha -/-$ Photoreceptors

The Tr$\alpha -/-$ photoreceptors were light adapted with continuous backgrounds. The Tr$\alpha -/-$ receptors sensitivity already started dropping when they were exposed to considerably dimmer backgrounds compared to WT cones. Again, the sensitivity-intensity data does not seem to fit to the Weber function. The decrease in sensitivity seems to taper off at the brightest backgrounds used. Thus, the contribution of pigment bleaching does not seem to be significant. Moreover these results indicate that the Tr$\alpha -/-$ photoreceptors do not behave in a WT cone manner.

There are also similarities between Tr$\alpha -/-$ and WT cone light adapted photoresponses (continuous background). The t_p seems to grow with incremental backgrounds. The same can be said for the recovery. τ_{rec}, however increases notably for Tr$\alpha -/-$ photoresponses while WT cone photoresponse values of τ_{rec} display no clear rise or fall in response to brighter background illumination.

All this data put together indicates that there is a serious alteration of cone phototransduction caused by deletion of the rod α-transducin gene. This suggests that rod transducin is present in cones and participating in cone phototransduction. The data also clearly indicates that the photoresponses obtained cannot originate from a photoreceptor that function in a WT rod manner. The photoresponses does instead seem have a mix of rod and cone characteristics. Without further investigation, electrophysiological as well as biochemical, it is impossible to map out the

exact cause or causes for the alteration of the Tr$\alpha - /-$ photoreceptor photoresponse.

Bibliography

[1] Oyster C. W., *Retina I:Photoreceptors and Functional Organization*. Electronic document. Page last modified on 2 October 2008. Referred to 7.10.2008. Available at: http://photobiology.info/

[2] Dowling J.E., *The Retina, an Approachable part of the brain*,The Belknap Press of Harvard University Press, 1987, vol. 8 p. 9–18.

[3] Gordon L. Fain, Hugh R. Matthews, M. Carter Cornwall, and Yiannis Koutalos Adaptation in Vertebrate Photoreceptors *Physiological Reviews ,* 2001, vol. 81 p. 117–151.

[4] Pugh E.N., Lamb T.D, Phototransduction in Vertebrate Rods and Cones: Molecular Mechanisms of Amplification, Recovery and Light Adaptation *Handbook of Biological Physics, Vol 3,Molecular Mechanisms in Visual Transduction,* Chapter 5, 1. ed. North Holland, Inc., 2000, p. 183-255

[5] Burns M.E. and Baylor D.A., Activation, Deactivation, and Adaption in Vertebrate Photoreceptor cells *Annual Reviews Neuroscience,* 2001, vol. 24 p. 779-805.

[6] Carter-Dawson L.D., and LaVail M.M. Rods and cones in the mouse retina *The Journal of Comparative Neurology* 1979, vol. 188 p. 245–262

[7] Tachibanaki S., Shimauchi-Matsukawa Y, Arinobu D., and Kawamura S. Molecular Mechanisms Characterizing Cone Photoresponses. *Photochemistry and Photobiology,* 2006, vol. 83 p. 19–26

[8] Nikonov S.S., Kholodenko R., Lem J., and Pugh E.N. Jr. Physiological features of the S- and M-cone photoreceptors of wild-type mice from single-cell recordings. *Journal of General Physiology,* 2006, vol. 127 p. 359–374

[9] Heikkinen H., Nymark S., and Koskelainen A. Mouse cone photoresponses obtained with electroretinogram from the isolated retina. *Vision Research,* 2008, vol. 48 p. 264–272

[10] Donner K., Hemilä S., Koskelainen A. Light adaptation of cone photoresponses studied at the photoreceptor and ganglion cell levels in the frog retina. *Vision Research,* 1998, vol. 38 p. 19–36

[11] Matthews H.R., Fain G.L., Murphy R.L., and Lamb T.D. Light adaptation in cone photoreceptors of the salamander: a role for cytoplasmic calcium. *Journal of Physiology,* 1990, vol. 420 p. 447–469

[12] *Anatomical image of the eye*, downloaded 5.8.2008. Available at: http://www.amdcanada.com/template.php?lang=eng&section=4&subSec=2d&content=4_2

[13] Tortora G. J. and Derrickson B., *Principles of Anatomy and Physiology* 11. ed. John Wiley & Sons, Inc., 2006, p. 582–591

[14] Rodieck R. W., *The First Steps in Seeing*, Sinauer Associates, 15.1.1998.

[15] Despopoulus A., Silbernagl S., *Color Atlas of Physiology* , Georg Thieme Verlag, 5. ed. New York 2003, p. 344–355

[16] Gouras P., Ekesten B., Why do mice have ultra-violet vision? *Experimental Eye Research*, 2004, vol. 79, p. 887–892

[17] Despopoulus A., Silbernagl S., *Color Atlas of Physioilgy,* , Georg Thieme Verlag, 5. ed. New York 2003, p. 348-349

[18] Kilpeläinen, P. Trichromacy. Electronic document. Page last modified on 4 February 2008. Referred to 16.3.2008. Available at: http://en.wikipedia.org/wiki/Trichromacy

[19] Nawy S., Jahr C. E. Suppression by glutamate of cGMP-activated conductance in retinal bipolar cells. *Nature,* 1990, vol. 346 p. 269-271

[20] Rispoli G., Navangione A., and Vellani V. Transport of K+ by Na(+)-Ca2+, K+ exchanger in isolated rods of lizard retina. *Biophysical Journal,* 1995, vol. 69 p. 74–83

[21] Mann M. D., *The Nervous System In Action*. Electronic document. Page last modified on 28 April 2003. Referred to 2.5.2008. Available at: http://www.unmc.edu/Physiology/Mann/mann4b.html

[22] Mallery C., *Sensory Physiology*. Electronic document. Page last modified on 16 August 1999. Referred to 6.10.2008. Available at: http://porpax.bio.miami.edu/~cmallery/150/neuro/senses.htm

[23] *Phototransduction.* Electronic document. Page last modified on 25 March 2008. Refered to 2.5.2008. Available at: http://en.wikipedia.org/wiki/Visual_phototransduction

[24] Kennedy BN, Goldflam S, Chang MA, Campochiaro P, Davis AA, Zack DJ, Crabb JW Transcriptional Regulation of Cellular Retinaldehyde-binding Protein in the Retinal Pigment Epithelium. *The Journal of Biological Chemistry ,* 1998, p. 5591–5598.

[25] Tinker A. The selective interactions and functions of regulators of G-protein signaling. *Seminars in Cell & Developmental Biology 17,* 2006, p. 377–382.

[26] Krispel C.M., Chen D., Melling N., Chen Y-J.,Martemyanov K. A., Quillinan N., Arshavsky A. Y., Wensel T.G, Chen C-K, and Burns M.E. RGS Expression Rate-Limits Recovery of Rod Photoresponses. *Neuron,* 2006, vol17 p. 409–416.

[27] Malmivuo J., Plonsey R. Electroretinogram *Bioelectromagnetism-Principles and Applications of Bioelectric and Biomagnetic Fields* Oxford University Press, New York 1995, Chapter 28.4

[28] Granit R. The components of the retinal action potential in mammals and their relation to the discharge in the optic nerve. *Journal of Physiology,* 1933, vol. 77 p. 207–239.

[29] Wässle H. Parallel processing in the mammalian retina. *Neuroscience,* 2004, vol. 5 p. 1–11.

[30] Xu X, and Karwoski C.J. The origin of slow PIII in frog retina: Current source density analysis in the eyecup and isolated retina *Visual Neuroscience,* 1997, vol. 14 p. 827–833.

[31] Xu X, and Karwoski C.J. Current source density analysis of retinal field potentials. II. Pharmacological analysis of the b-wave and M-wave.*Journal of Neuroscience,* 1994, vol. 72 p. 96–105.

[32] Tomita T, and Yanagida T. Origin of the ERG Waves *Vision Research,* 1981, vol. 21 p. 1703–1707.

[33] Vinberg F., Strandman S and Koskelainen A. The Nose Component in Mammalian ERG , 2008, Manuscript

[34] Calvert P.D.,Krasnoperova N.V., Lyubarsky A.L., Isayama T., Nicolo M., Kosaras B., Wong G., Gannon K.S., Margolskee R.L., Pugh E.N. Jr., Makino C.L., and Lem J. Phototransduction in Transgenic Mice After Targeted Deletion of the Rod Transduction α-subunit *PNAS,* 2000, vol. 97 p. 13913–13918.

[35] Matthews H.R., Effects of lowered cytoplasmic calcium concentration and light on the responses of salamander rod photoreceptors *Journal of Physiology,* 1995, vol. 96 p. 267–286.

[36] Kawamura S., Murakami M., Calcium dependent regulation of cyclic GMP phosphodiesterase by a protein from frog retinal rods. *Nature,* 1991, vol. 349 p. 420–423.

[37] Matthews H.R., Hisatomi O., Kayada S., Tokunaga F, and Kuo C.H. Recoverin has S-modulin activity in frog rods. *Journal of Biological Chemsitry,* 1993, vol. 268 p. 14579–14582.

[38] Gordovikova E.N., Gimelbrandt A.A., Senin I.I., and Phillipov P.P., Recoverin mediates the calcium effect upon rhodopsin phosphorylation and cGMP hydrolysis in bovine retina rod cells *FEBS Lett.,* 1994, vol. 349 p. 187–190.

[39] Sagoo M.S., Lango L., G-protein deactivation is rate-limiting for shut-off of the phototransduciton cascade *Nature,* 1997, vol. 389 p. 392–395.

[40] Elias R.V., Sezate S.S., Cao W., and McGinnis J.F., Temporal kintetics of light/dark translocation and compartmentation of arrestin and α-transducin in mouse photoreceptor cells. *Molecular Vision,* 2004, vol. 10 p. 672–81.

[41] Nymark S, Haldin C, Tenhu H, and Koskelainen A., A new method for measuring free drug concentration: Retinal tissue as a biosenor. *Investigative Ophthalmology & Visual Science,* 2006, vol. 47 p. 2583–2588.

[42] Steinberg R.H.,Oakley B II, and Niemeyer G., Light-Evoked Changes in $[K^+]_o$ in Retina of Intact Cat Eye *Journal of Neurophysiology,* 1980, vol. 44 p. 897–921.

[43] Hughes B.A. and Takahira M., Inwardly Rectifying K Currents in Isolated Human Retinal Pigment Epithelial Cells *Investigative Ophthalmology & Visual Science,* 1996, vol. 37 p. 1125–1139.

[44] Frewerda J.A., Pattananik S.N., Shirley P. and Greenberg D.P., A Model for Visual Adaptation for Realistic Image Synthesis. Electronic document. Refered to 22.7.2008. Available at: http://www.graphics.cornell.edu/pubs/1996/FPSG96.html.

[45] Burns ME, Lamb TD. Visual Transduction by Rod and Cone Photoreceptors In Visual Neurosciences MIT Press. Cambridge, MA. USA, 2003, p. 215–233.

[46] Burns ME, Arshavsky VY. Beyond Counting Photons: Trials and Trends in Vertebrate Visual Transduction *Neuron ,* 2005, vol. 48, p. 387–401.

[47] Pepperberg D.R., Cornwall M.C.,Kahlert M., Hofman K.P.,Jin J. Jones G.J. and Ripps H. Light-dependent delay in the falling phase of the retinal rod photoresponse *Visual Neuroscience,* 1992, vol. 8 p. 9–18.

[48] Nymark S., Heikkinen H, and Koskelainen A. Frog cone light adaptation. *Manuscript*, 2008,

[49] Silva G.A., Hetling J.R., Pepperberg D.R. Dynamic and steady-state light adaptation of mouse rod photoreceptors in vivo *Journal of Physiology*, 2001, vol. 534 p. 203–216

[50] Nymark S., Heikkinen H, Haldin C., Donner K., and Koskelainen A. Light responses and light adaptation in rat retinal rods at different temperatures *Journal of Physiology*, 2005, p. 923–938

[51] Soo F. S. , Detwiler P.B., and Rieke F Light Adaptation in Salamander L-Cone Photoreceptors *The Journal of Neuroscience*, 2008, vol. 28 p. 1331–1342